

DESY HERA 1986-11

July 1986

Eigentum	der	DESY	Bibliothek
Property of			library
Zugang:	0 4.	SEP 1986	
Accessions:			
Leihfrist:	7	Tage	
Loan period:		days	

DESY III : DESIGN REPORT

DESY III Group

Editor: J.R.Maidment

R A L

mit noch im Archiv vorhanden



DESY behält sich alle Rechte für den Fall der Schutzrechtserteilung und für die wirtschaftliche Verwertung der in diesem Bericht enthaltenen Informationen vor.

DESY reserves all rights for commercial use of information included in this report, especially in case of filing application for or grant of patents.

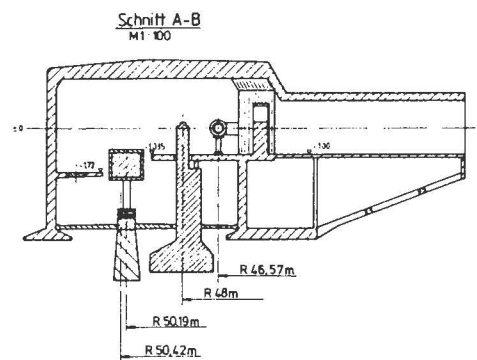
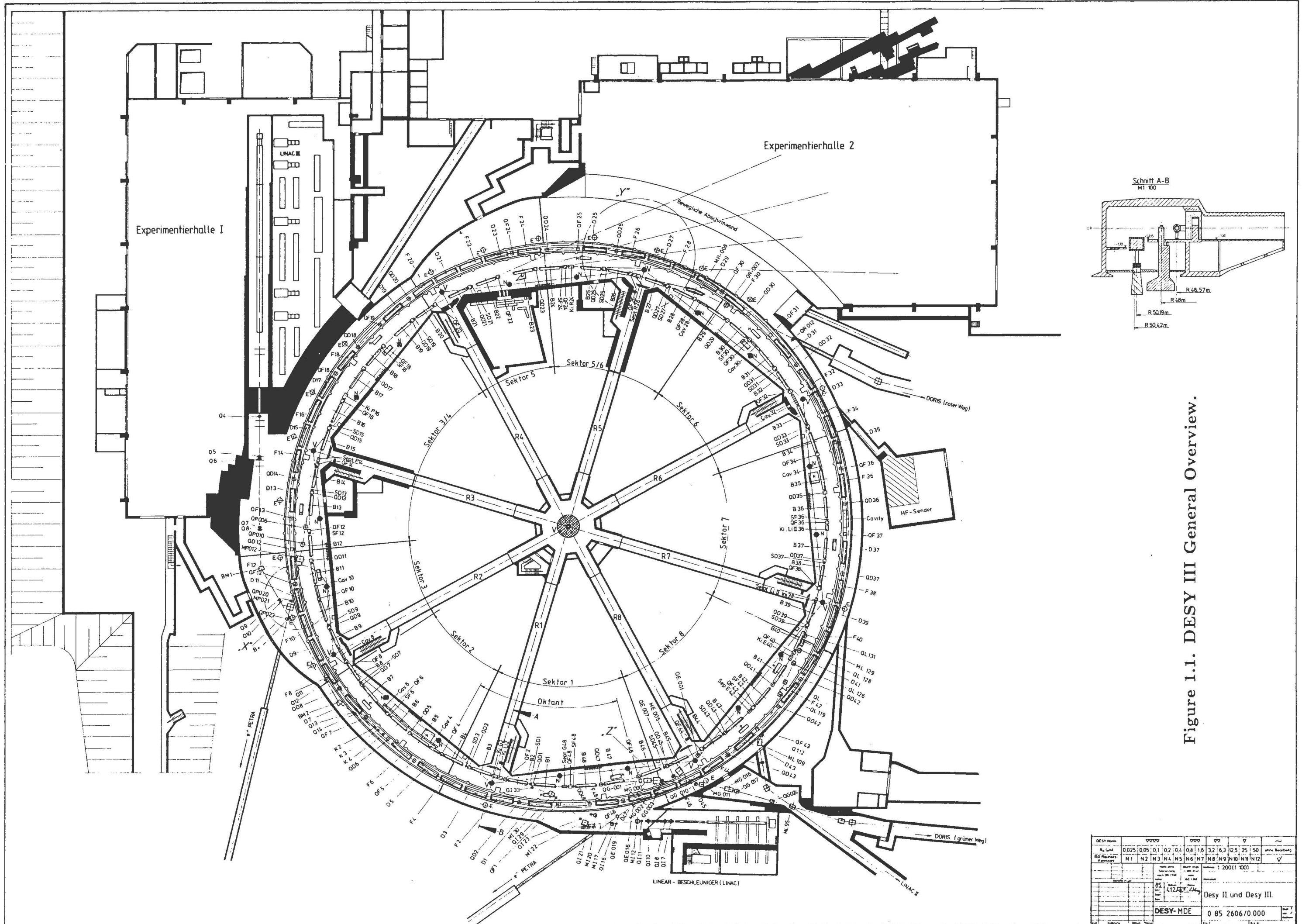


Figure 1.1. DESY III General Overview.

DESY Name	0000	0001	0002	0003	0004	0005	0006	0007	0008	0009	0010	0011	0012	0013	0014	0015	0016	0017	0018	0019	0020	0021	0022	0023	0024	0025	0026	0027	0028	0029	0030	0031	0032	0033	0034	0035	0036	0037	0038	0039	0040	0041	0042	0043	0044	0045	0046	0047	0048	0049	0050	0051	0052	0053	0054	0055	0056	0057	0058	0059	0060	0061	0062	0063	0064	0065	0066	0067	0068	0069	0070	0071	0072	0073	0074	0075	0076	0077	0078	0079	0080	0081	0082	0083	0084	0085	0086	0087	0088	0089	0090	0091	0092	0093	0094	0095	0096	0097	0098	0099	0100	0101	0102	0103	0104	0105	0106	0107	0108	0109	0110	0111	0112	0113	0114	0115	0116	0117	0118	0119	0120	0121	0122	0123	0124	0125	0126	0127	0128	0129	0130	0131	0132	0133	0134	0135	0136	0137	0138	0139	0140	0141	0142	
-----------	------	------	------	------	------	------	------	------	------	------	------	------	------	------	------	------	------	------	------	------	------	------	------	------	------	------	------	------	------	------	------	------	------	------	------	------	------	------	------	------	------	------	------	------	------	------	------	------	------	------	------	------	------	------	------	------	------	------	------	------	------	------	------	------	------	------	------	------	------	------	------	------	------	------	------	------	------	------	------	------	------	------	------	------	------	------	------	------	------	------	------	------	------	------	------	------	------	------	------	------	------	------	------	------	------	------	------	------	------	------	------	------	------	------	------	------	------	------	------	------	------	------	------	------	------	------	------	------	------	------	------	------	------	------	------	------	------	------	------	------	------	------	------	--

DESY III: DESIGN REPORT

DESY III Group

Editor: J.R.Maidment

Preface

This report is an attempt to collect in one document information on both the conceptual design and engineering implementation of the DESY III proton injector for the HERA project. Unfortunately it is an almost invariable fact that a report of this type is, in part, obsolete when printed. Nevertheless it is hoped that it may serve as a useful reference description.

The authors, a complete list of whom may be found below, would like to acknowledge many useful discussions with members of other institutes. In particular the help of many colleagues at CERN and Rutherford is greatly appreciated. The editor would like to thank Frau M. Stuckenberg for much patience in typing parts of the manuscript and also Frau M. Möller for preparing some of the illustrations.

List of Authors

E. Bakewicz,	W. Bothe,	L. Criegee,
D. Degèle,	W. Ebeling,	A. Febel,
A. Gilgrass*,	H.R. Heller,	G. Hemmie,
H.F. Hoffmann,	E. Karantzoulis,	O. Kaul,
H. Krause,	J.R. Maidment**,	H. Narciss,
F. Peters,	W. Radloff,	J. Rümmler,
G. Sandels**,	N. Schirm,	K. Sinram,
H.P. Wedekind,	B.H. Wiik,	K. Wille***.

* Dept. of Nuclear Physics, Oxford University, UK.

** RAL, Chilton, UK.

*** Present address: Dortmund University.

Contents

1	Introduction.	2
2	Lattice Design.	4
3	Performance Limits.	9
4	Magnets.	13
5	Injection.	19
6	Ejection.	21
7	RF System.	28
8	Vacuum System.	35
9	Diagnostics.	40
10	Power Supplies.	42
11	Controls.	45
12	Construction.	46
13	References	56

1 Introduction.

The proton injection path for HERA consists of:

- a) The H^- linac ($p_{max} = 0.31 \text{ GeV/c}$).
- b) The DESY III synchrotron ($p_{max} = 7.5 \text{ GeV/c}$).
- c) The PETRA II machine ($p_{max} = 40 \text{ GeV/c}$).
- d) HERA.

The DESY III synchrotron, described in this report, is a proton accelerator with a cycle time of ~ 4 seconds. Protons are accumulated using multi-turn charge exchange injection from the linac. The circulating beam is formed into 11 bunches which are accelerated to 7.5 GeV/c , extracted in a single turn and transferred to PETRA. This process is repeated several times to accumulate bunches in PETRA. The beam is then accelerated in PETRA to 40 GeV/c and transferred into the HERA main ring. The complete scheme is repeated until the full complement (210) of bunches are stored in HERA. The final HERA bunch spacing is established in DESY III and maintained throughout the subsequent injectors.

When considering alternative designs for DESY III one main requirement was that as much use as possible be made of existing buildings and equipment. In particular, since the present DESY I electron accelerator is being replaced, one goal was to make use of the DESY magnets and to install the new proton accelerator in the existing synchrotron building.

Figure 1.1. shows a plan view of the magnet arrangement within the synchrotron hall, the reference numbers used to identify each magnet are based on those at present defining the DESY I arrangement. They are adhered to throughout this report.

2 Lattice Design.

The present DESY I lattice consists of 24 symmetric FODO cells with combined function magnets of effective length 4.15 m separated by 2.45 m. The betatron tunes are ~ 6.25 in both planes and $\gamma_t \sim 5.6$. The proton accelerating cavity, see Section 7, requires a greater free space than that provided by the present lattice as does the injection system. Further, to preserve the longitudinal beam density in a slow cycling machine in which the particles cross transition would require a sophisticated additional pulsed quadrupole system. ^[1] The lattice design of DESY III embodies long straight sections and avoids the need to cross transition by providing a transition energy greater than the peak design energy.

Figure 2.1. shows the magnet structure and lattice functions of the chosen optics. The ring consists of 8 such superperiods, the combined function magnets being grouped together to yield one long straight per octant. There are 4 additional quadrupoles per octant which serve to adjust the dispersion function and hence the transition energy, as well as allowing some flexibility in the choice of betatron tunes. Table 2.I lists some of the basic parameters of the synchrotron.

Table 2.I DESY III Parameters

1. General

Nominal Circumference	316.799	m
Injection Momentum	310.19	Mev/c
Extraction Momentum	7.50	GeV/c
Cycle Time	3.6	s
Total No. of Protons	1.125×10^{12}	

2. Lattice

No. of Superperiods	8	
Total no. of Long Straights	8	
Length of Long Straight	5.54	m
Betatron Tune(H/V)	5.90/4.82	
Gamma(transition)	8.77	
Maximum Beta(H)	19.4	m
Maximum Beta(V)	20.3	m
Maximum Dispersion	4.25	m
Linear Chromaticity (H/V)	-6.14/-5.82	

A complete list of the optical structure and envelope parameters may be found in Table 2.II. The value of the lattice functions tabulated apply at the end of each individual element.

Table 2.II DESY III Optics

Number of Superperiods = 8
Individual Elements

	LENGTH	ANGLE	KV VALUE
BF	4.150000	0.130900	-0.068760
BD	4.150000	0.130900	0.070014
QF	0.580000	0.0	-0.539750
QD	0.580000	0.0	0.436800
QF1	0.580000	0.0	-0.124400
QD1	0.580000	0.0	0.083500
D72	0.720000	0.0	0.0
D41	0.410000	0.0	0.0
D57	0.570000	0.0	0.0
D185	1.850000	0.0	0.0
D554	5.540000	0.0	0.0

SUPERPERIOD STRUCTURE

BF,D72,QD,D554,QF,D72,BD,D185,QD1,D41,
BF,D72,BD,D72,BF,D72,BD,D57,QF1,D41:

		DX	DX'	BETAX	ALFAX	MUX/2PI	BETAZ	ALFAZ	MUZ/2PI	ELTOT
0		1.604	0.327	11.163	-0.715	0.0	9.213	1.035	0.0	0.0
1	BF	2.081	-0.121	6.068	1.406	0.067	13.661	-2.500	0.074	4.150
2	D72	1.994	-0.121	4.297	1.053	0.090	17.536	-2.882	0.081	4.870
3	QD	2.070	0.388	3.789	-0.134	0.113	18.278	1.666	0.086	5.450
4	D554	4.219	0.388	13.518	-1.622	0.254	6.159	0.522	0.174	10.990
5	QF	4.060	-0.928	12.956	2.532	0.261	6.740	-1.582	0.188	11.570
6	D72	3.392	-0.928	9.606	2.120	0.271	9.288	-1.957	0.203	12.290
7	BD	1.254	-0.202	5.500	-0.767	0.392	13.806	1.345	0.251	16.440
8	D185	0.880	-0.202	9.325	-1.301	0.434	9.525	0.969	0.277	18.290
9	QD1	0.774	-0.162	11.225	-2.005	0.443	8.225	1.252	0.287	18.870
10	D41	0.707	-0.162	12.945	-2.189	0.449	7.251	1.124	0.296	19.280
11	BF	0.022	-0.134	14.517	1.975	0.488	9.026	-1.708	0.402	23.430
12	D72	-0.074	-0.134	11.848	1.732	0.497	11.712	-2.021	0.413	24.150
13	BD	-0.498	-0.090	12.184	-1.843	0.565	13.536	1.774	0.456	28.300
14	D72	-0.562	-0.090	15.025	-2.103	0.574	11.140	1.554	0.466	29.020
15	BF	-0.313	0.197	13.707	2.282	0.612	12.377	-1.961	0.536	33.170
16	D72	-0.171	0.197	10.656	1.956	0.621	15.404	-2.243	0.544	33.890
17	BD	1.008	0.426	8.103	-1.115	0.712	14.498	2.365	0.580	38.040
18	D57	1.250	0.426	9.463	-1.272	0.722	11.949	2.106	0.587	38.610
19	QF1	1.469	0.327	10.600	-0.659	0.732	10.099	1.127	0.596	39.190
20	D41	1.604	0.327	11.163	-0.715	0.738	9.213	1.035	0.603	39.600

AVERAGE RADIUS = 50.420 TOTAL ANGLE=360.0 QX = 5.900 QZ = 4.821
GAMMA TRANSITION = 8.770724

The sensitivity of the lattice to variations in the quadrupole currents is shown in Table 2.III. This is a matrix relating changes in tune and γ_t to fractional changes in the current in each of the four quadrupole circuits. The change in betatron tune resulting from a 5% change in each of the quadrupole strengths is plotted in Figure 2.2.

TABLE 2.III Lattice Sensitivity

ΔQ_x	2.56	-0.79	0.31	-0.31	$\Delta K/K_F$
ΔQ_z	-1.12	3.05	-0.37	0.27	$\Delta K/K_D$
$\Delta \gamma_t$	52.3	-8.68	1.02	-0.28	$\Delta K/K_{F1}$ $\Delta K/K_{D1}$

The required aperture is calculated from the specification ^[2] of the linac output parameters taking into account that shortly after the start of acceleration the peak momentum spread increases to $\Delta p/p \sim \pm 2.7 \times 10^{-3}$. The horizontal aperture is taken to be a linear addition of the betatron and synchrotron oscillation amplitudes.

The chosen dimensions of the vacuum chamber - Section 8 - allow for about twice the specified emittance with a safety factor everywhere of ± 5 mm for closed orbit distortions. Vertically, however the available F-sector gap height - Section 4 - allows twice the nominal emittance with a reduced closed orbit safety factor of ± 2 mm.

Installation tolerances are specified by assuming that initially a reduced emittance beam ($\sim 10\%$) is injected and that with a 95 % probability it will remain within the vacuum chamber. These are detailed in Table 2.IV where rms displacements horizontally (δx), vertically (δz) and longitudinally (δs) together with rms rotation about the longitudinal axis ($\delta \alpha_s$) are specified.

TABLE 2.IV RMS Installation Tolerances

	Quads	Bending Magnets	
δx	0.32	0.18	mm
δz	0.34	0.18	mm
δs	-	4.0	mm
$\delta \alpha_s$	-	0.42	mrad

Specification of injection element tolerances is based on restricting emittance growth due to errors to $\leq 10\%$. Similarly the reproducibility demanded of the extraction and transfer to PETRA ensures emittance growth, both transverse and longitudinal of $\leq 20\%$. This then leads to tolerances on individual elements such as kickers - Section 6 - and field stability - Section 10.

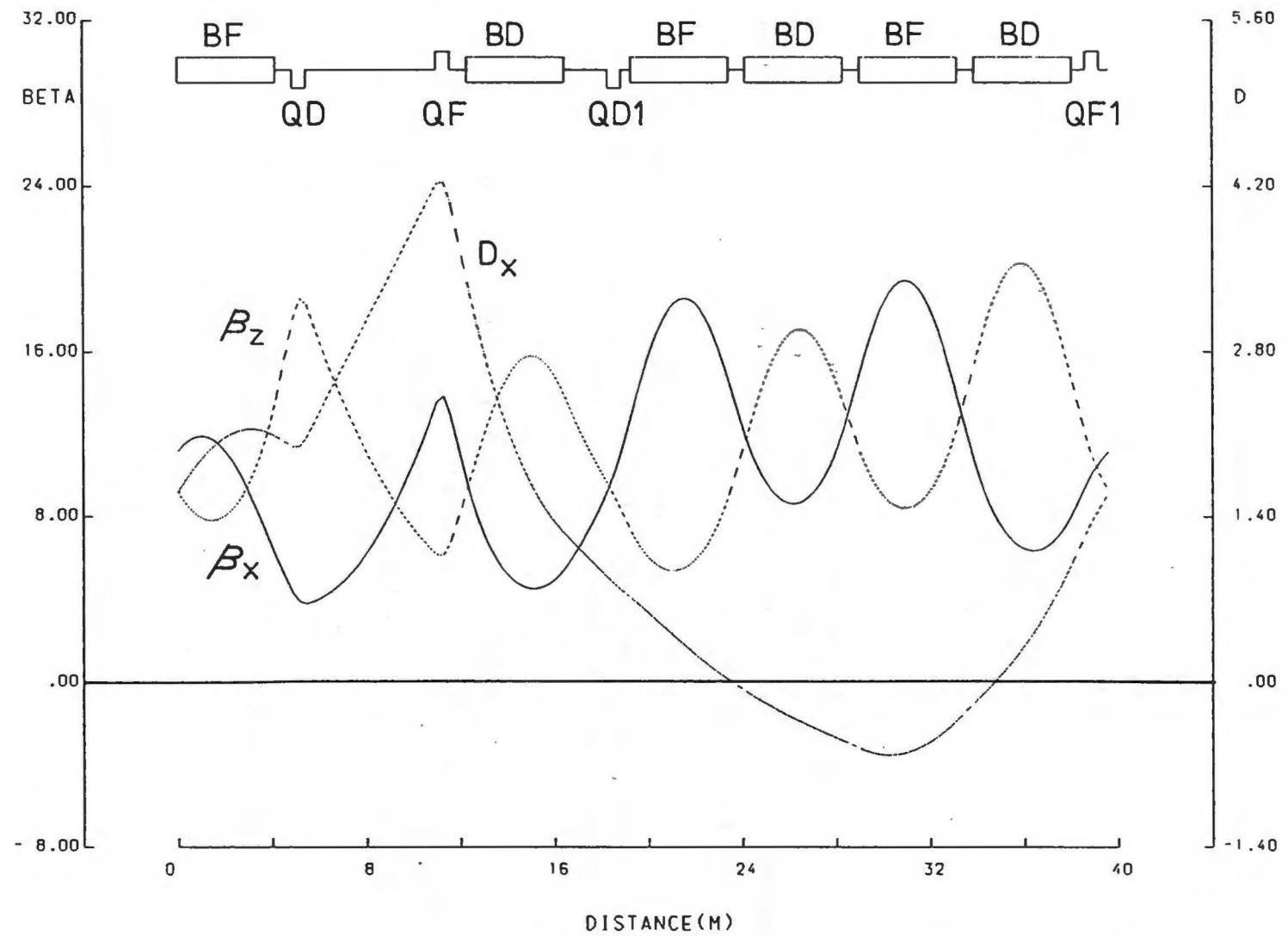


Figure 2.1. Nominal Optic.

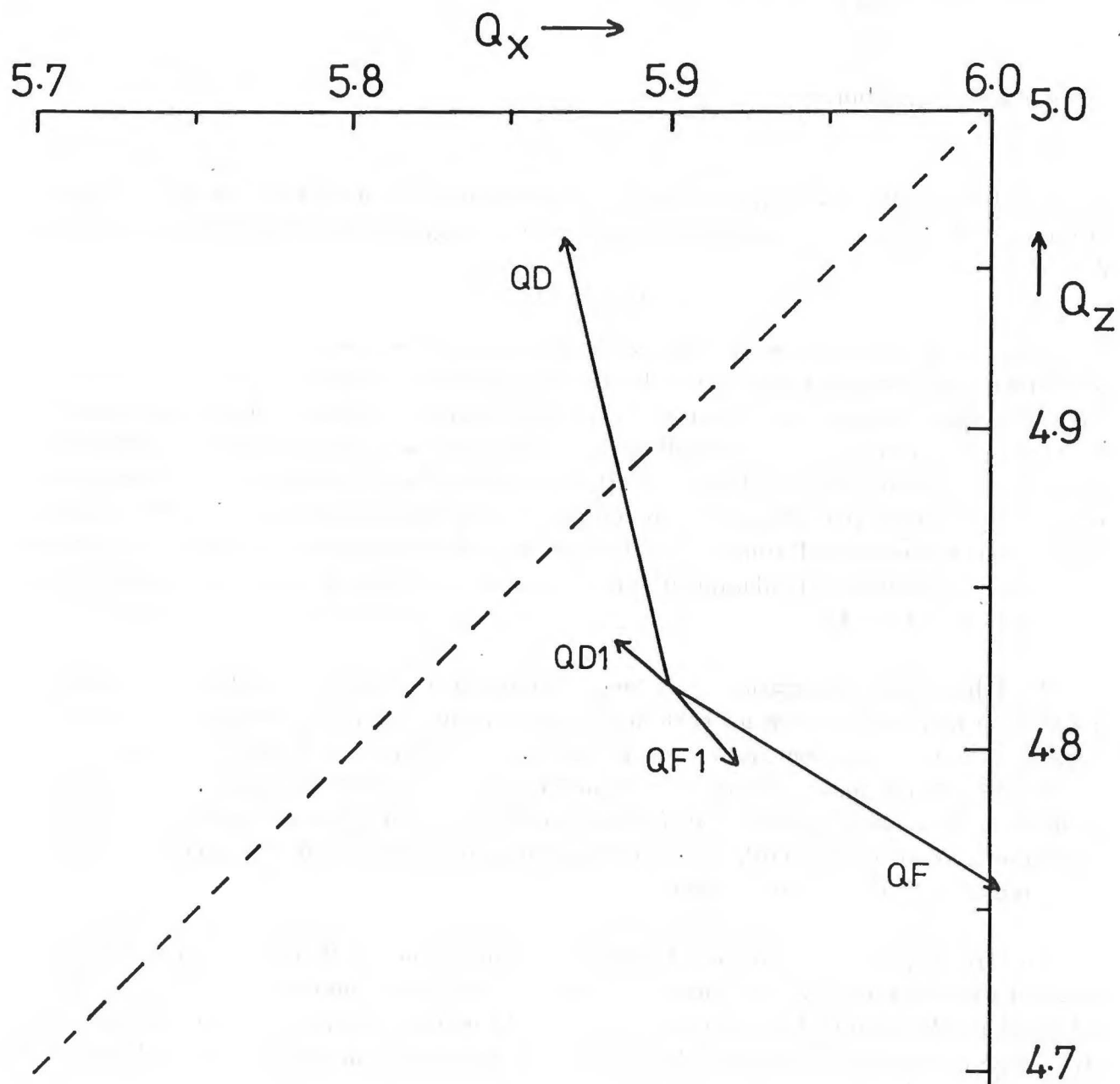


Figure 2.2. Tune Shift for 5% Quad. Change.

3 Performance Limits.

Single Particle Instabilities

These instabilities may arise when there is resonance between the betatron oscillations of the particles and the harmonic components of the magnetic guide field. This can happen if

$$nQ_x + mQ_z = p$$

where n, m, p are integers. In a Q_x versus Q_z diagram these equations represent straight lines and the nominal working point is chosen to avoid resonances of low order. At low energy, transverse space charge forces produce a spread of incoherent betatron frequencies and the working point becomes an area overlapping a number of low order resonances. Figure 3.1 shows ^[3] the working diagram for DESY III with the working area shown at 3 different times in the acceleration cycle. Region A corresponds to the situation at injection; B shows the maximum expected spread, some 20 ms after the start of acceleration; C illustrates the spread after ~ 0.5 s at which and subsequent times the area required is a region notionally free of resonances of order ≤ 4 .

A preliminary investigation ^[4], using a version of the particle tracking code RACE-TRACK ^[5] modified to allow for both non-relativistic motion and acceleration, of the transverse acceptance reduction due to non-linearities in the guide field, has been made. The non linear bending magnet fields were represented by a random distribution of multipole coefficients of standard deviation 10% of their mean value. The mean values were obtained by fitting to data derived both from old model measurements and from recent preliminary measurements ^[6] of 2 existing magnets.

To sample possible incoherent tunes within the beam, tracking was performed for 3 different working points; the nominal optic and 2 others whose tunes are indicated in Figure 3.1 by II and III. Optic II is close to the crossing of many 4th order resonances whilst optic III is close to many of 3rd order. All tracking was done with the inclusion of a closed orbit deviation around the ring of rms value 1 mm.

The non-linear transverse acceptance is given by that particle amplitude which just remains within the aperture during the whole acceleration cycle and is most conveniently quoted as a fraction of the linear acceptance given by the aperture alone. In these terms the results may be summarised as follows:

Working Point	Fractional Stable Acceptance
Nominal	0.55
II	0.70
III	0.25

It was also noted that if the nominal tune was shifted away from the nearby skew sextupole driven resonance $2Q_x - Q_z = 7$ the stable acceptance increased to 65% of the linear.

These results cannot be simply interpreted for the time varying distribution of incoherent tunes is unknown. In any event the linear acceptance provided by the aperture (Section 2) is a factor of two greater than the injected emittance. We intend to use multipoles (Section 4) to allow correction of some of the most serious resonances and have scheduled a program of magnet field measurement (Section 12) to enable correction strengths to be calculated.

Coherent Instabilities

a) Longitudinal

i) Microwave Instability

This instability occurs if the longitudinal emittance of a beam of a given intensity is too small. We may write the criterion ^[7] for the allowed longitudinal impedance as:

$$\left| \frac{Z}{n} \right| \leq \frac{1}{21} \frac{h}{I} \left(\frac{\epsilon_L c}{R} \right)^{3/2} \left| \frac{ne}{E} \right|^{3/4} (V h \cos \varphi_s)^{1/4}$$

with I the circulating current, E the total energy of the beam and ϵ_L the longitudinal emittance. The longitudinal impedance divided by the mode number ($\frac{Z}{n}$) has a negative imaginary space charge term and a positive imaginary inductive wall term:

$$\frac{Z}{n} = j \left(\Omega_0 L - \frac{g_0 Z_0}{2\beta\gamma^2} \right)$$

where Z_0 is the free space impedance, g_0 is a geometric coupling factor and Ω_0 is the revolution frequency. The value of the effective wall inductance depends upon the smoothness of the vacuum chamber, the number of steps and incidental cavities (e.g. kickers, monitors etc.) that are installed. The wall impedance is independent of energy and in general in the range of a few to few tens of ohms, but the space charge term is proportional to γ^{-2} , being $\sim 1 \text{ k}\Omega$ at injection and $\sim 6\Omega$ at full energy. At injection the allowed impedance is some $7 \text{ k}\Omega$ and at top energy $\sim 10\Omega$. At top energy the wall and space charge contributions may be comparable and although some cancellation occurs we must still estimate the expected wall impedance.

The impedance due to a step may be estimated from ^[8]

$$\left| \frac{Z}{n} \right| \simeq \frac{Z_0}{2} (S - 1)^2 \frac{h_l}{\pi R}$$

where $S = \frac{h_t}{h_l}$, the ratio of the half heights of the vacuum chamber. For the proposed DESY III vacuum chamber with some 30 steps we estimate that:

$$\left| \frac{Z}{n} \right| \simeq 0.5 \text{ ohms}$$

The contribution of a kicker to the wall impedance comes from its resistive part which is given by [9]:

$$Z_r = \frac{Z_0}{4}(1 - \cos kl)$$

with Z_0 the characteristic impedance of the kicker, l the length of the module and $k = \frac{8\pi^2}{Z_0} \frac{b}{a} f \cdot 10^{-7}$; a and b are the gap half height and width respectively. Using the proposed extraction kickers parameters we estimate $Z_r \simeq 3$ ohms. Although we have no data at present to allow estimates of the impedances of other discrete devices (e.g. injection bump magnets, diagnostics etc.) it is not expected that these will give a contribution such that the total wall impedance becomes $> 16\Omega$. We therefore expect the beam to be stable with respect to microwave blow-up at all energies.

ii) Coupled-bunch Instabilities

The computer code BBI [10] has been used to study these instabilities. The code requires input of the impedances in the form of single resonators (up to 3 allowed) which are described by a resonant frequency, shunt impedance and quality factor Q . The effect of all the accidental cavities was represented by a broad-band resonator, $Q=1$, with resonant frequency of ~ 1.3 GHz -the vacuum pipe cut-off frequency. An additional resonator representing the fundamental of the rf-cavity was used. No data exists describing the higher longitudinal modes of the cavity.

The broad-band resonator, which gives rise to the inductive wall effect at low frequencies, can cause an instability through the loss of Landau damping. This is the case in DESY III for $t \geq 1$ s due to the fact that the bunch is relatively short compared with the rf wavelength and thus there is a very small spread in the synchrotron frequency with amplitude. However the growth times calculated are of the order of $\sim 10^5$ s.

The combined effect of broad-band + cavity resonators gives growth times of the order ≥ 400 s. BBI finds no unstable multibunch modes driven by the cavity alone, however the combined effect of both broad-band and cavity resonators does lead to some unstable multibunch modes. In the worst case growth times are ≥ 10 s. We thus conclude that with the available information on longitudinal impedances we expect no problems from either single or multi-bunch instabilities. All are either stable or have growth times sufficiently long compared with the acceleration time.

b) Transverse Instabilities

The broad-band transverse resonator for BBI is scaled from that used in the longitudinal case by the factor $\frac{2R}{h^2}$ where h is the half height of the vacuum chamber. No data is available on higher deflecting modes of the rf-cavity. As expected for a machine operating below transition energy, the rigid mode of the transverse head-tail effect is stable with the natural negative chromaticity. No unstable higher single bunch modes were predicted by BBI. This was also the case when resistive wall effects were included. Multibunch instabilities, driven by specific deflecting modes could not be investigated but are not expected to cause problems.

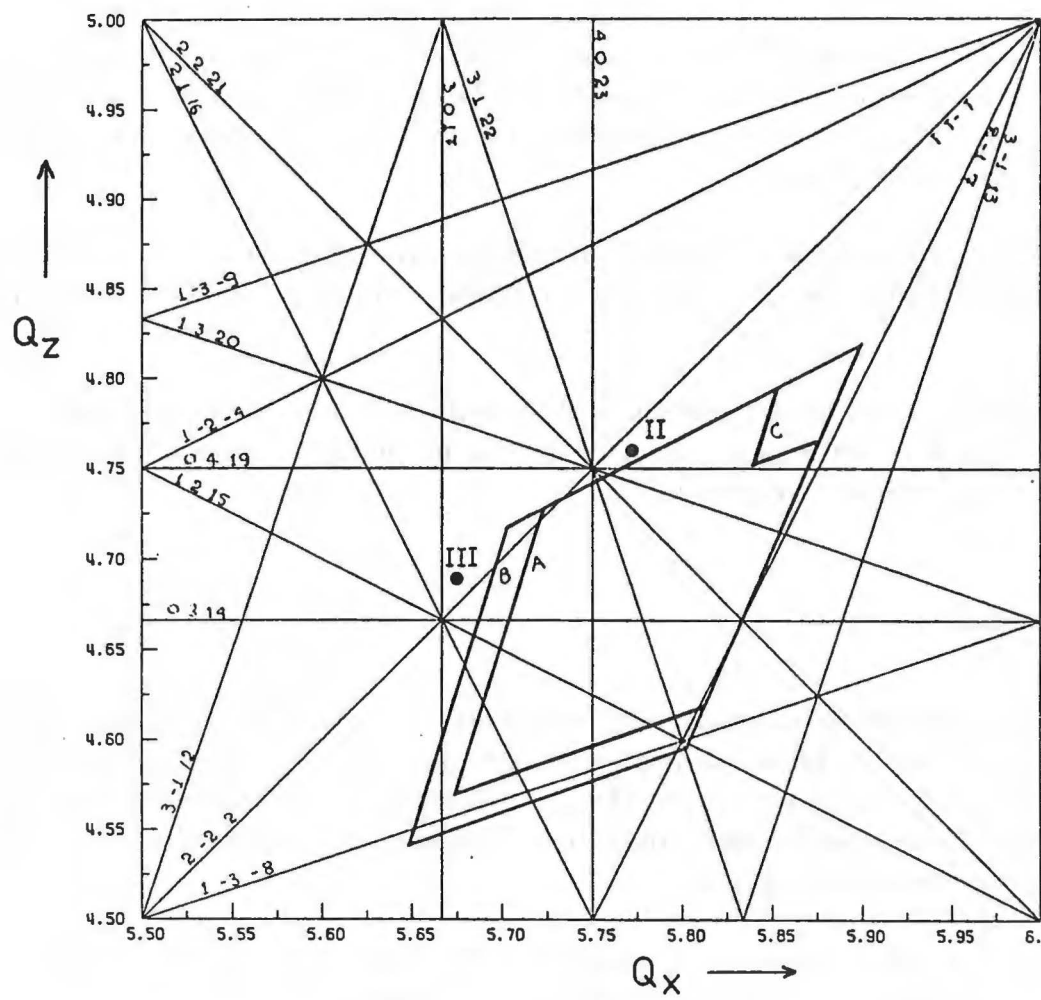


Figure 3.1. Tune Diagram.

4 Magnets.

The magnet system consists of a combination of separated and combined function units. The 360° of bending is achieved by using the combined function sector magnets of the DESY I synchrotron. The additional focussing needed to obtain high γ_t is provided by 32 quadrupoles similar to the DESY II type.

Emittance dilution by nonlinear fields will be corrected by means of 8 multipole magnets at present installed in DESY I. These units contain sextupole, octupole and skew quadrupole coils.

Horizontal closed orbit correction will be performed using back-leg windings on the F-sectors powered by DC power supplies rated at 10 Amps. For vertical correction 24 DC powered C-type dipoles are installed.

a. Dipoles

No major modifications need to be made to the majority of the magnets taken over from DESY I except for the boring through the yokes of some D-sectors as outlined in Section 8. Because of the slow cycling operation ($\dot{B}_{max} \sim 0.53 \text{Ts}^{-1}$) the self induced voltage drop is small compared with their present 50 Hz operation. They are thus connected in series and powered by a single, programmable supply.

Figure 4.1. shows the cross-section of the focussing sector and Figure 4.2. shows that for the defocussing sector. Table 4.I below lists the main parameters.

Table 4.I Bending Magnet Parameters

Magnetic length		l_m	4.15	m
Bending radius		ρ	31.7023	m
Focussing strength	F-sector	K_F	0.068760	m^{-2}
Focussing strength	D-sector	K_D	-0.070014	m^{-2}
Field at ejection (7.5 GeV/c)		\hat{B}	0.789	T
Field at injection (0.31 GeV/c)		B_i	0.0326	T
Current at 7.5 GeV/c		\hat{I}	1250	A
Rate of magnet field rise		\dot{B}	0.525	T/s
Number of coil windings		N_F	28	
		N_D	44	
Resistance per magnet		R_F	11.8	$\text{m}\Omega$
		R_D	17.7	$\text{m}\Omega$
Inductance per magnet		L_F	21.4	mH
		L_D	36.2	mH

b. Quadrupoles

There are 32 quadrupoles similar to those in DESY II. The cross-section is identical but the end field shaping is modified to simplify manufacture. Since \dot{B} is about 40 times smaller than in DESY II no eddy current field distortions will occur. The quadrupoles are excited by four independent circuits fed by four parallel tracking power supplies. Figure 4.3. shows the cross-section, the parameters being listed in Table 4.II.

Table 4.II Quadrupole Parameters

technical data	DESY III - Quadrupole	
max. field gradient	16.91	T/m
core length	580	mm
total length	696	mm
total weight	1150	kg
weight of coil	37	kg
coil cross-section	2393	mm ²
conductor cross-section	217.5	mm ²
turns n/coil	11	—
resistance at 20°C	6.96	m Ohm
inductance	3.4	mH
peak current	1530	A
effective current	937	A
current density	4.31	A/mm ²
power losses	6.11	kW
number of cooling channels	1 per magnet	—
water flow	2.19	l/min
δt cooling water	40	°K
differential pressure	1.9	bar

c. Multipoles

Eight multipole magnets each containing sextupole, octupole and skew quadrupole windings will be taken over from DESY I. They will be used to compensate betatron resonances due to non-linear field particularly at injection. Initially they will be powered with existing DC supplies, keeping open the option to upgrade them to track the acceleration cycle. Figure 4.4. shows the multipole cross-section and Table 4.III details their parameters.

Table 4.III Multipole Parameters

Overall length flange to flange	635	mm
Core length	435	mm
Cylinder length including connections	500	m
Overall diameter	260	mm
Effective magnetic length	400	mm
Orientation:		
octupole	normal	water cooled
sextupole	normal	water cooled
quadrupole	twisted by 45°	air cooled
Max. currents		
sextupole and octupole	800	A (rms)
quadrupole	85	A (rms)
Fields		
sextupole	$\frac{d^2 B}{dx^2} \left[\frac{T}{m^2} \right] = 3.23 \times 10^{-2} \times I[A]^{measured}$	
octupole	$\frac{d^3 B}{dx^3} \left[\frac{T}{m^3} \right] = 1.6 \times I[A]^{calculated}$	
quadrupole	$\frac{dB}{dx} \left[\frac{T}{m} \right] \sim 2 \times 10^{-3} \times I[A]^{calculated}$	

d. Orbit Correction

Data from the position monitors will be used to derive an excitation table for the correction coils. Each is independently powered and is capable of steering the beam over the full aperture at injection. Figure 4.5. shows the azimuthal distribution of monitors and correctors over two octants.

The high energy orbit will be corrected by transversely displacing a few quadrupoles. It is expected that the procedure will only be performed once per year or less.

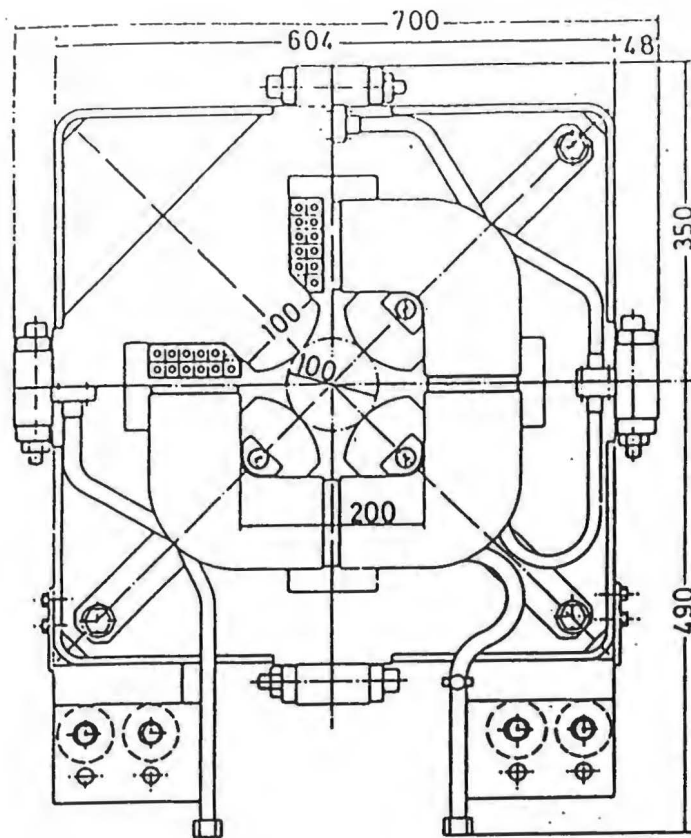


Figure 4.3. Quadrupole Cross-section.

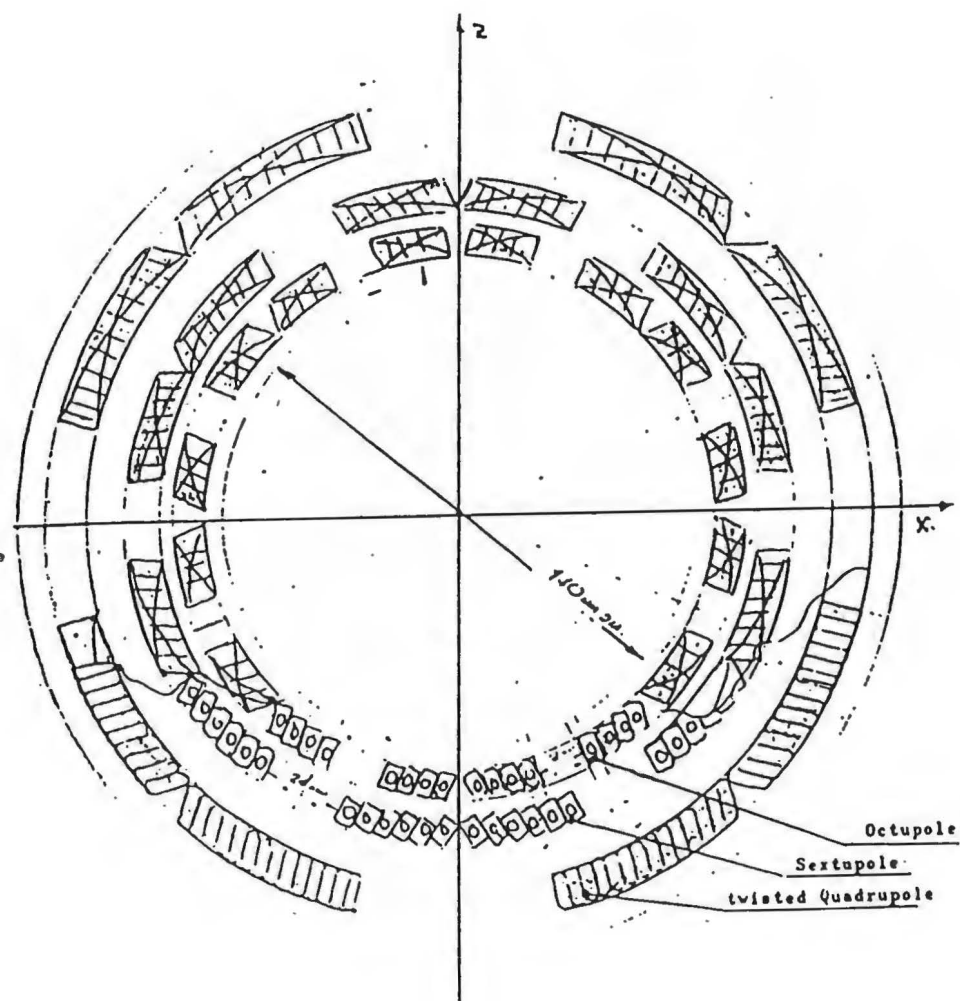


Figure 4.4. Multipole Cross-section.

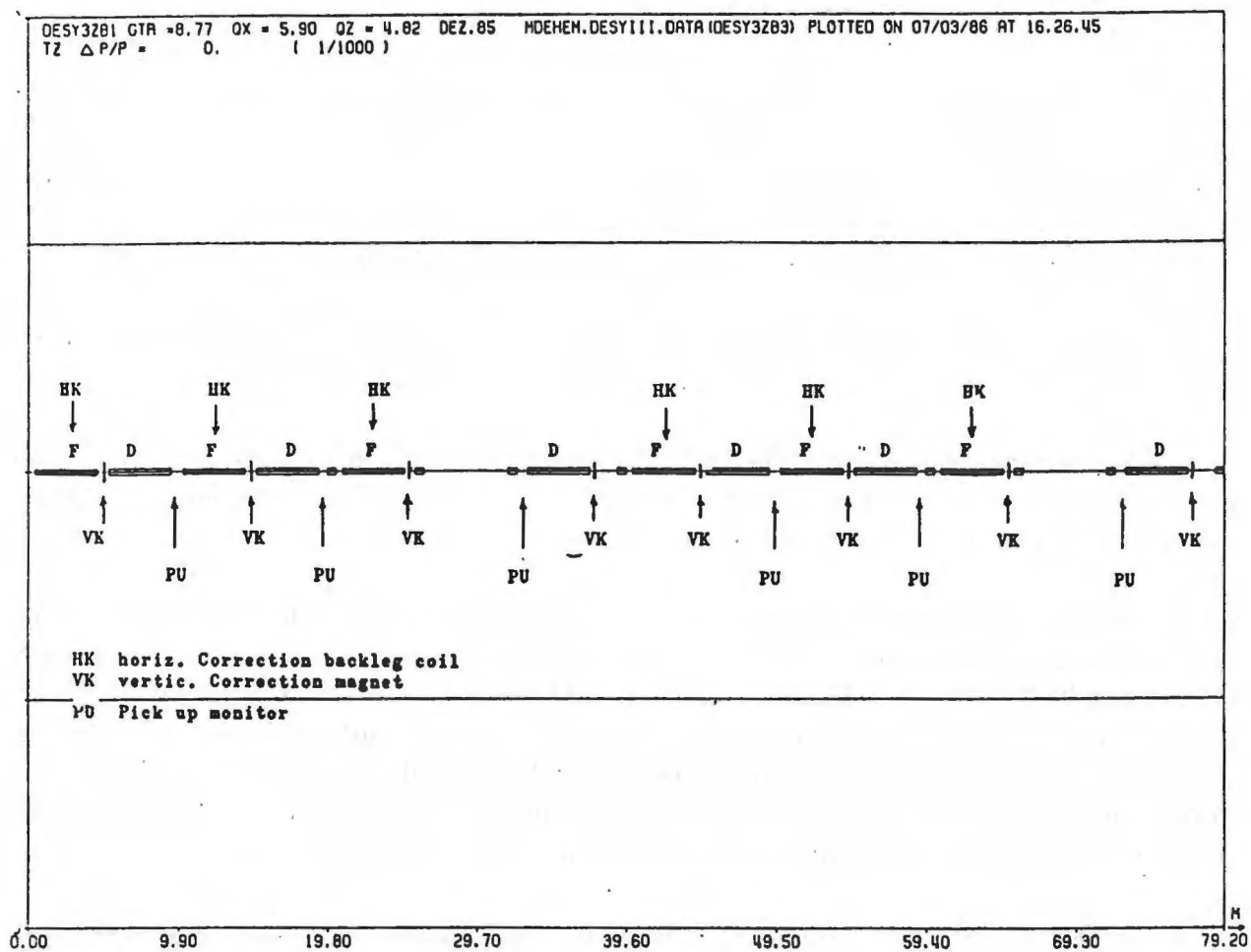


Figure 4.5. Distribution of Monitors and Correctors

5 Injection.

H^- ions from the 50 MeV linear accelerator are injected by means of a septum magnet and bump magnet system located entirely in one long straight section. The H^- ions are converted to protons by a thin foil through which also passes the circulating beam. Using this technique protons may be accumulated without, in principle, transverse phase space dilution. Up to ten turns corresponding to $\sim 35 \mu s$ may be injected.

The general layout of the injection system is shown in Figure 5.1. It is located in the straight section between QF7 and QD6 and requires a free length of 3.9m.

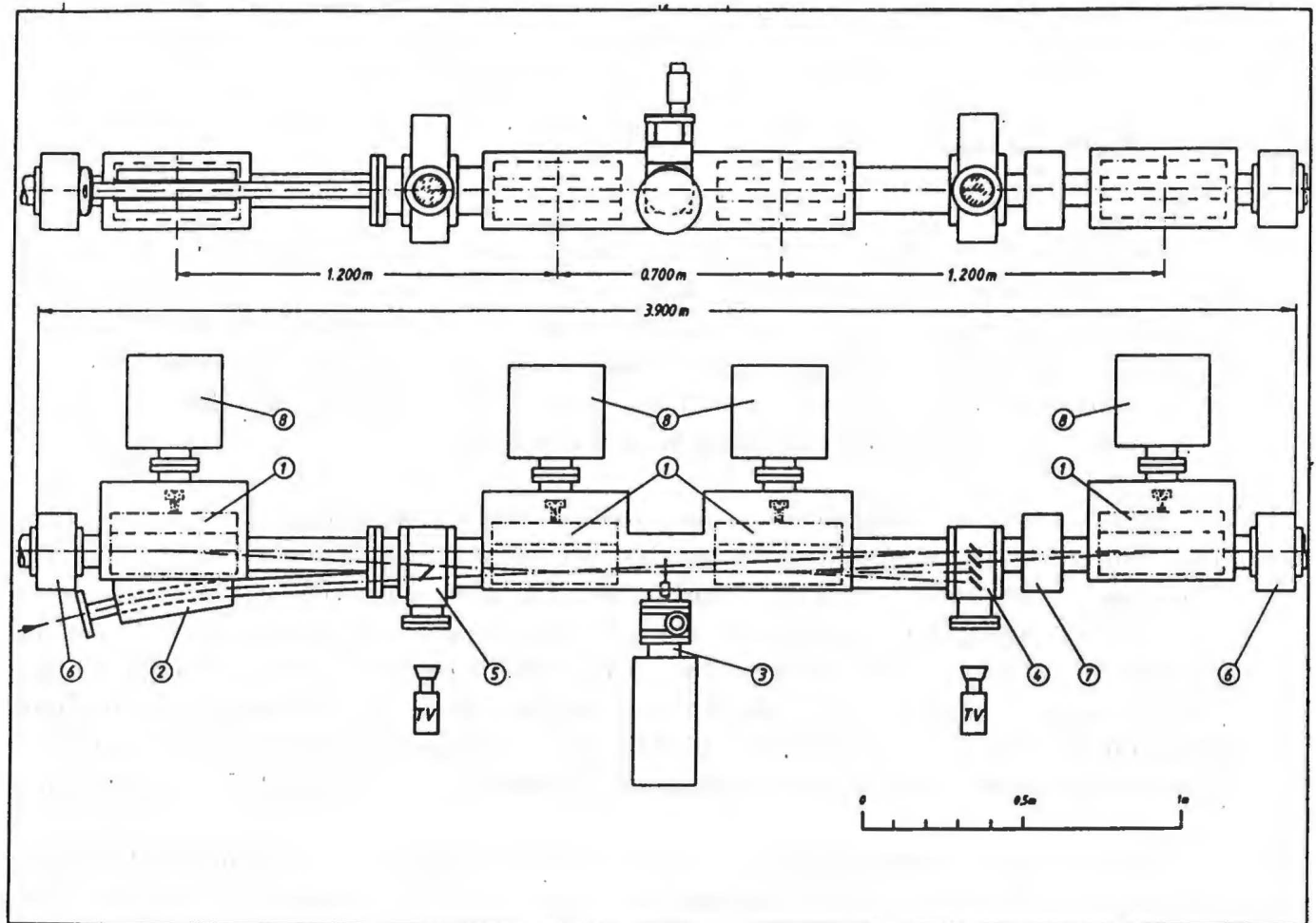
At the injection foil, which is located 0.4m downstream of the midpoint of the straight the matched beam width is 30 mm and the height is 34 mm. The horizontal bump amplitude is 60 mm with a pulse to pulse stability of ± 0.8 mm.

The DC powered septum magnet provides a 200 mrad deflection whilst each of the bump magnets should give 50 mrad. Preliminary field calculations based on a C-magnet design using the PE2D code ^[11] have been made. Assuming 8C11 ferrite is used the flux density $B = 0.132$ T, total length = 400 mm, field homogeneity $\Delta B/B = 2.10^{-4}$ and inductance $L = 0.85 \mu H$. However realisation of this design with standard available ferrite sizes results in a larger than wanted volume and a consequent increase in the inductance per unit to $\sim 1.3 \mu H$. Further calculations using 3H2 ferrite aimed at reducing the volume are in progress.

The pulser is designed to provide a bump duration of $35 \mu s$ with a rather slow rise time and a fall time of about $30 \mu s$. The voltage needed depends upon the total inductance which is assumed to be $7 \mu H$ comprising $2 \mu H$ for 100 m of cable, $1.6 \mu H$ for bus bars and $4 \times 0.85 \mu H$ for the magnets. Using thyristors the pulser will deliver 6000 Amp at a voltage of 2 kV. The resulting fall time is then such that the emittance growth due to foil traversal by the circulating beam will be $\leq 10\%$.

The stripping section is based on a simplified version of that in use at RAL. The stripper is Al_2O_3 foil $55 \text{ mm} \times 55 \text{ mm}$ and of thickness $30 \mu g/cm^2$ supported by a U-shaped aluminium frame. There is a remote controlled foil change mechanism containing 5 spare foils. Foil fabrication is carried out in a special chemical laboratory.

Special diagnostics to allow set-up and monitoring of operation are contained within the system. Position monitors are located both upstream and downstream whilst following the first bump magnet there is a profile monitor and a mirror to allow visual foil inspection. Between the third and fourth magnet is a glass scintillator with 4 addressable fixed positions for monitoring circulating beam position, bumped beam position, H^+ and H^- components. Upstream of the fourth magnet is a current monitor. An electron catcher is installed in the foil box to prevent overheating by stripped electrons.



- | | |
|---|--|
| ① KICKER MAGNET 50 MRAD | ⑤ POS. MONITOR AND VISUAL FOIL CONTROL |
| ② SEPTUM MAGNET 200 MRAD | ⑥ POSITION MONITOR |
| ③ FOIL CHANGE MECHANISM WITH AN ELECTRON CATCHER FOR STRIPPED ELECTRONS | ⑦ CURRENT MONITOR (TOROID) |
| ④ POSITION MONITOR (GLASS SCINTILLATOR) FOR MONITORING: | ⑧ ION PUMP 400 L/s |
| - INJECTION MAGNET | |
| - BEAM ORBIT | |
| - H_o | |
| - H_- | |
| ALSO H_o , H_- BEAM DUMP | |

Figure 5.1. Injection System Layout.

6 Ejection.

The beam is extracted horizontally in a single turn and transferred into matched rf buckets in PETRA. To do this a fast kicker and pulsed septum magnet system is used. The nominal gap between the tail of one bunch and the head of the adjacent one is ~ 89 ns, however to ease kicker requirements and to allow for the possible use of one of the 11 bunches as a diagnostic bunch, we extract only 10 bunches the remaining one being deflected during kicker field rise on to an absorber upstream of the septum.

Initially the circulating beam is displaced radially at the septum azimuth by a slow beam bump derived by powering the back-leg windings on three F-sectors adjacent to the extraction straight (F12, F14, F16). After correct synchronisation with PETRA the beam is kicked across the septum by means of two fast kickers, one situated in the medium straight immediately upstream of the septum, the other in the long straight of the upstream octant. The kickers are separated in horizontal betatron phase by $\sim 190^\circ$ the one in the medium straight being some 60° in phase upstream of the septum. Figure 6.1. illustrates the transverse beam displacements at the septum entrance and Figure 6.2. shows the kicked beam envelope.

The deflection needed per kicker is ~ 1.6 mrad. The kickers are transmission line units terminated in their characteristic impedance. Figure 6.3. is a schematic of the PFN and kicker. Each unit is designed to provide the required kick with a safety factor of $\sim 20\%$, Table 6.I. is a list of the main parameters. Figures 6.4. and 6.5. show respectively a cross-section of the magnet and a detail of the top view.

Table 6.I Kicker Magnet Data

No. of units	2	
Ferrite length	1.0	m
Gap height	56	mm
Magnetic field	48	mT
Pulse current	2.14	kA
Pulse voltage	22	kV
Pulse duration	1	μ s
PFN voltage	44	kV
Kicker filling time	130	ns
Impedance	10	Ohm

The ejection septum magnet has a 5 mm thick septum and is 1.3 m long. It deflects the extracted beam into the transport line to PETRA without the need for additional bending magnets, sufficient beam clearance being provided at the extraction straight downstream quadrupole QD12. Table 6.II details the main magnet parameters and Figure 6.6. shows the geometry in the region of the extraction point.

Table 6.II Ejection Septum Magnet Data

Bending angle	75.274	mrاد
Iron length	1.3	m
Peak current	17	kA
Field strength	1.4486	T
Chamber (w×h)	24×12	mm
Septum thickness	5	mm
Pulse duration	1.5	μs
Repetition time	3.6	s

A study of the additional quadrupoles which are needed to match the extracted beam optically into the transport channel has been made. The 3 quadrupoles are shown in Figure 6.6. Two (QPP2, QPP3) are already to hand whilst the remaining lens, QPP1, is identical with a type to be used in the PETRA-HERA transport line. The design of a beam-stop to enable DESY III to operate in test mode is currently in progress.

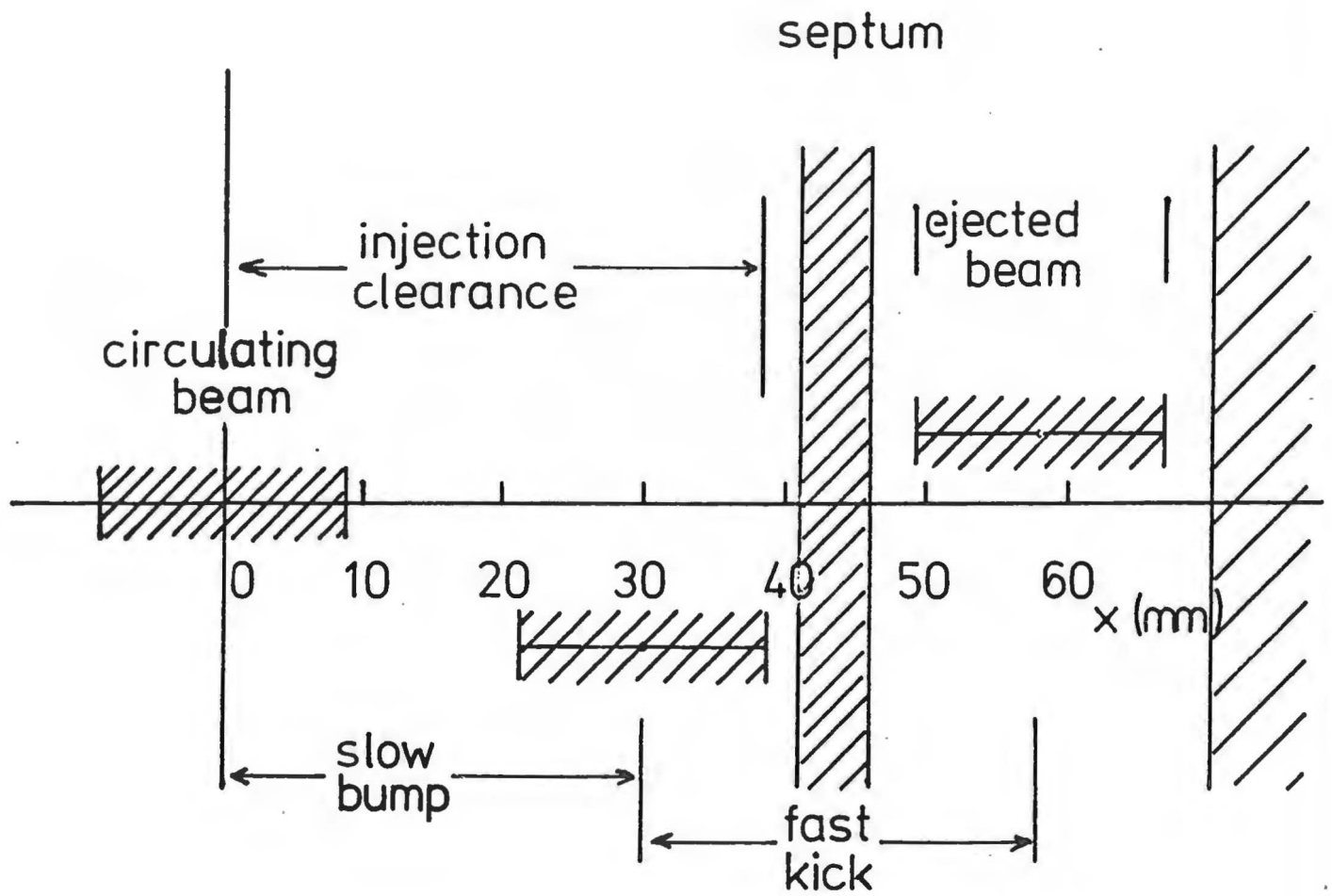


Figure 6.1. Beam Displacement at Septum.

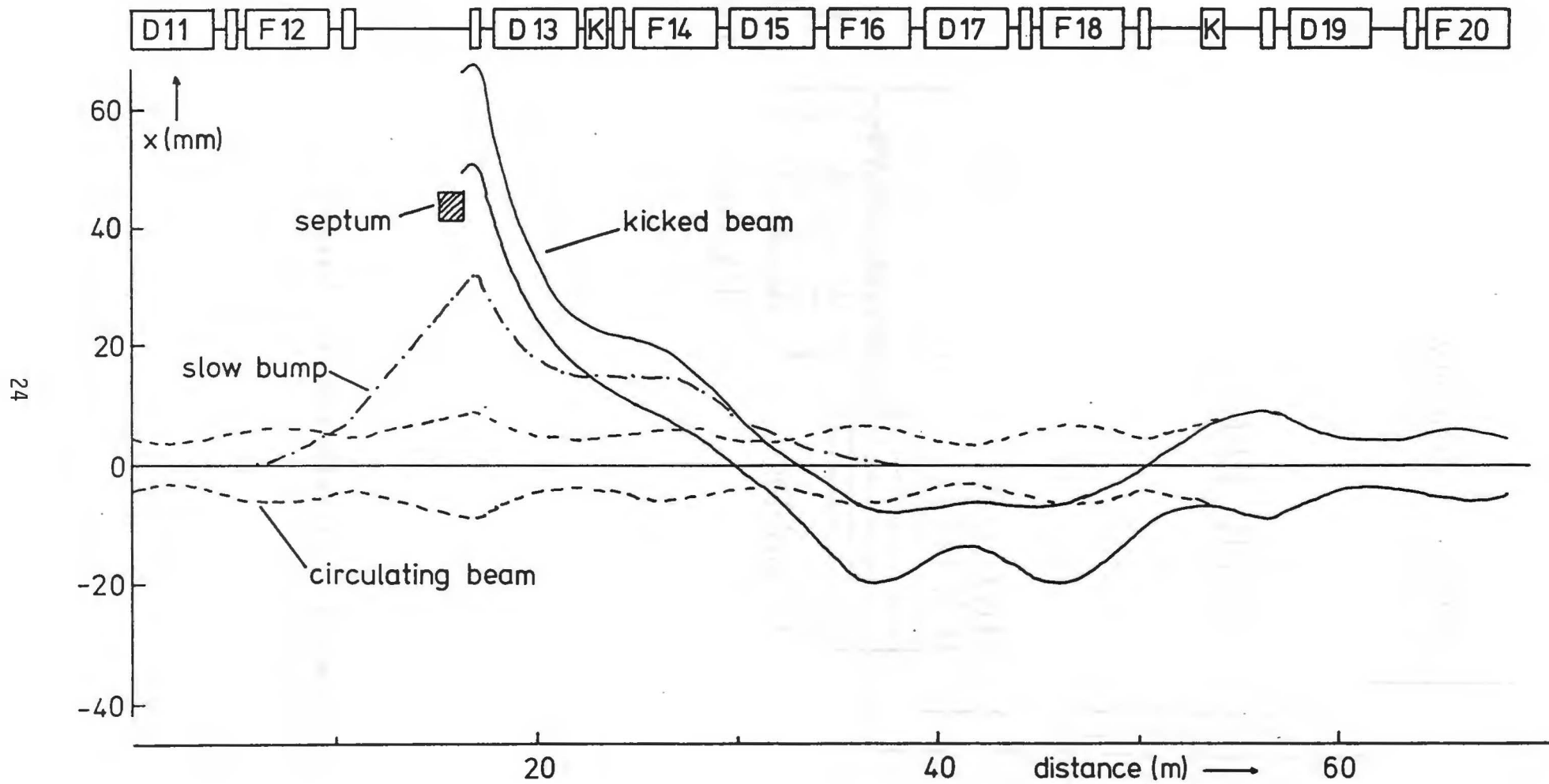


Figure 6.2. Beam Envelope at Extraction.

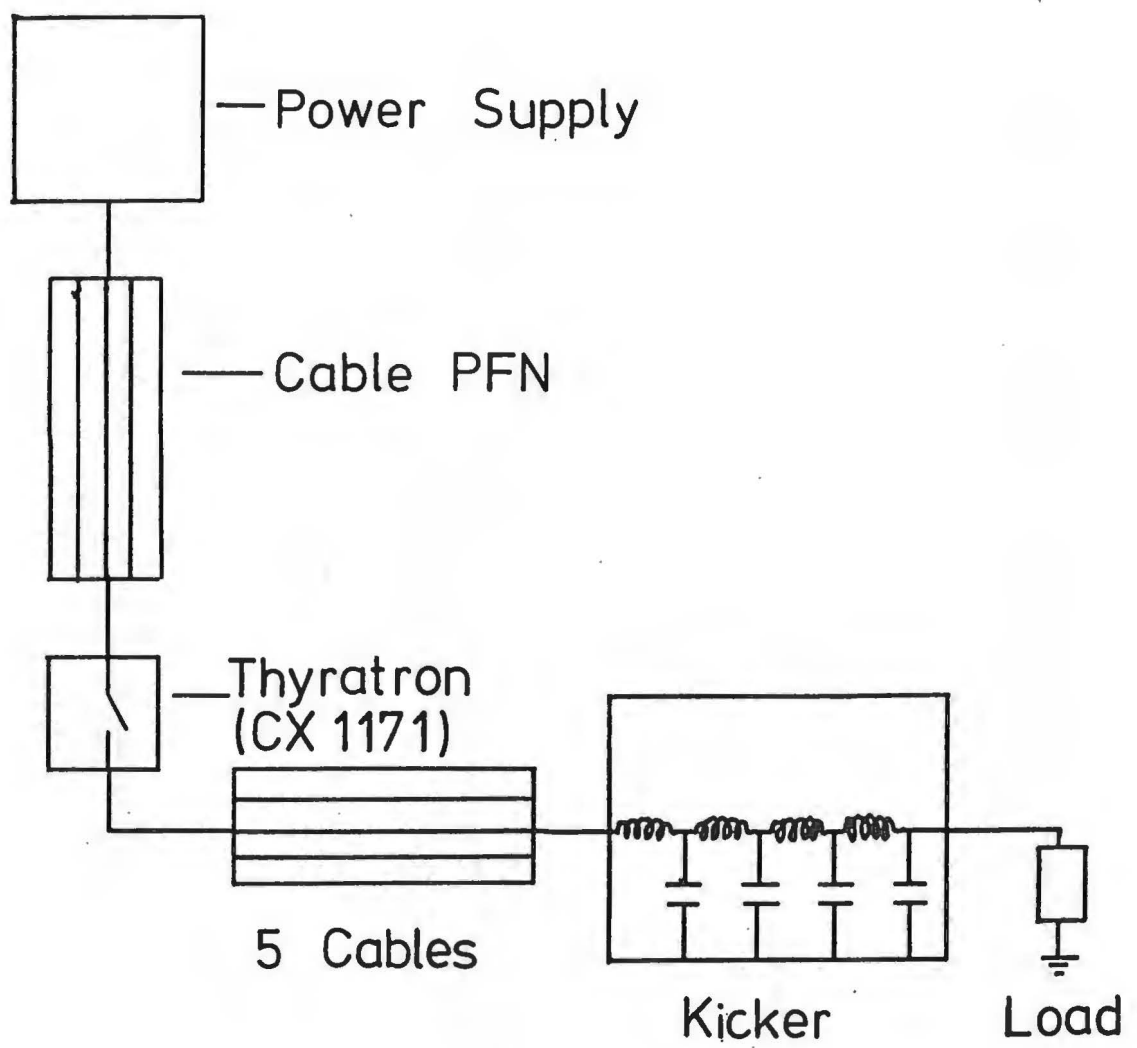


Figure 6.3. Extraction Kicker Layout.

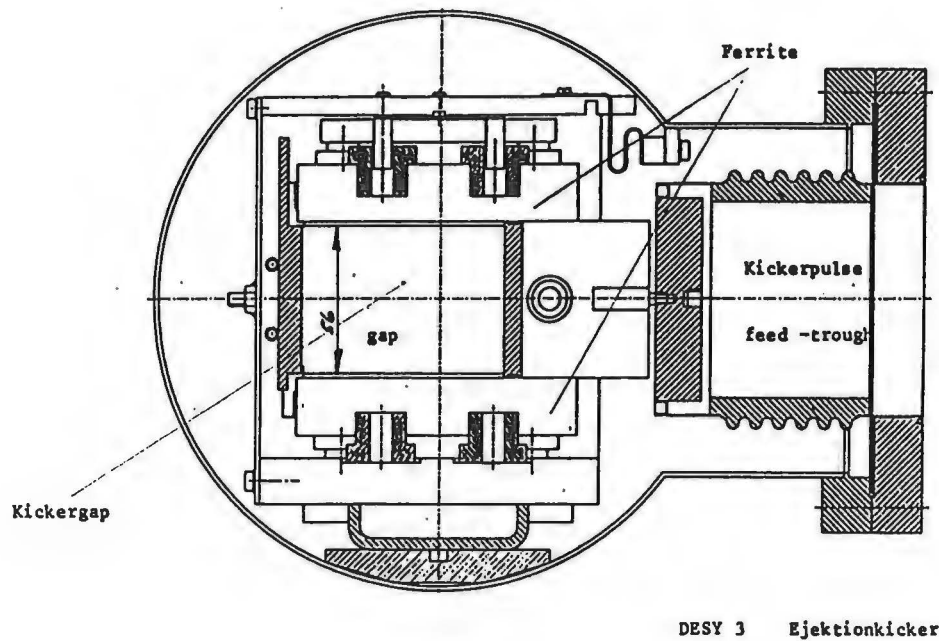


Figure 6.4. Ejection Kicker Cross-section

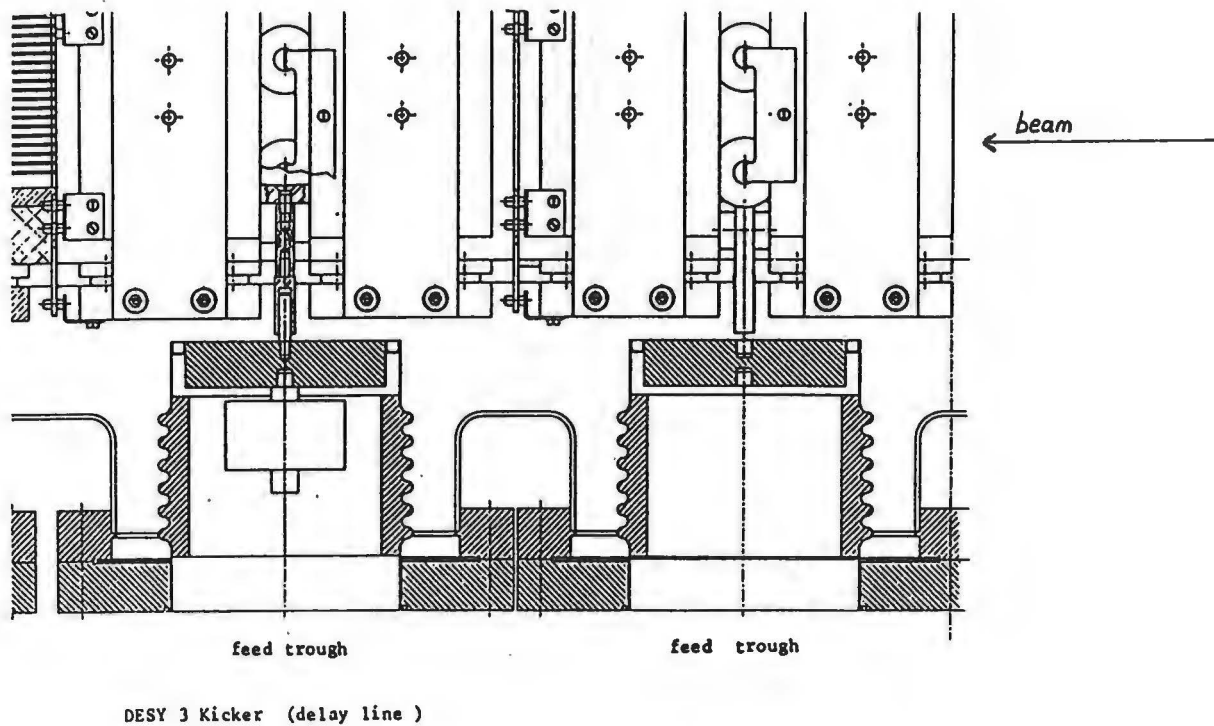


Figure 6.5. Ejection Kicker Plan View

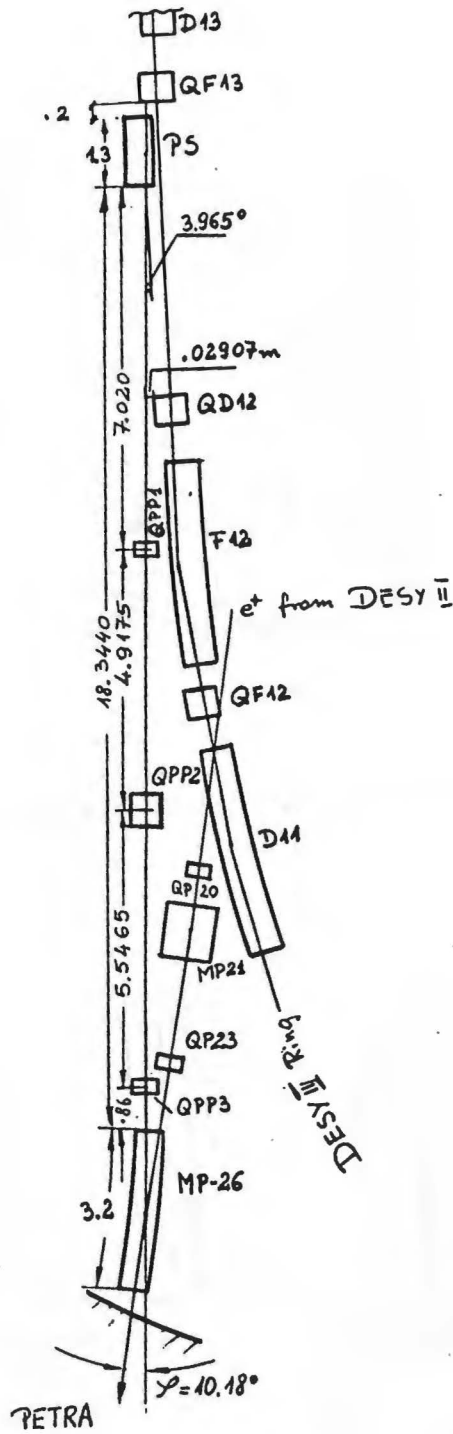


Figure 6.6. Extraction Beam Line

7 RF System.

To accelerate protons a radio frequency system is required comprising an accelerating cavity, an RF power amplifier chain, a low level swept frequency oscillator (VCO), a high current bias system to tune the cavity and a beam control system. Figure 7.1. shows a schematic of the complete system and Table 7.I gives the basic parameters.

Table 7.I RF System Parameters

Bunch phase space area	0.072	eVs
RF harmonic number	11	
Frequency at injection	3.27	MHz
Frequency stability at injection	$\pm 1 \times 10^{-4}$	
Frequency at extraction	10.33	MHz
Frequency stability at extraction	$\pm 2.5 \times 10^{-7}$	
Peak accelerating voltage	18	kV
Design value for peak voltage	20	kV
Cavity power dissipation (max)	40	kW
Maximum bias current	3000	A
Gamma at extraction	8.06	
Gamma(transition)	8.77	

The cavity is one of the spare PS units from CERN and consists of two quarter wavelength ferrite loaded resonators each with one ceramic gap. The power amplifier is housed in the support structure, the output tetrode being directly coupled to the cavity, see Figure 7.2. It is installed in the ring in a straight section near an experimental area, where all the required RF and biasing equipment is housed, Figure 7.3. The RF induction in the ferrites during the cycle varies between 45 Gauss and 23 Gauss as shown in Figure 7.4.

The amplifier chain consists of a pre-amplifier and final amplifier. It generates the cavity voltage amplitude versus time shown in Figure 7.5. The input signal level is 10 mW and the final amplifier delivers 40 kW (at maximum) into the cavity, resulting in an RF voltage of 10 kV per gap.

To tune the cavity over the required frequency range the bias applied to the ferrite is varied. To achieve this a high current power supply and associated high current transistor regulator is used. The regulated output current varies between 200 A and 2750 A as shown in Figure 7.6., with a period of the waveform of 3.6 s. The power supply provides a maximum current of 3000 A at an output voltage of 30 V. Peak ripple current is specified to be $\Delta I/I \leq 2.10^{-2}$.

Four control loops, as indicated in Figure 7.1. are necessary namely:

a. Tuning Loop

During acceleration the cavity frequency must be varied between 3.2 MHz and 10.3 MHz. The tuning loop adjusts the bias current and hence the cavity inductance to ensure that the fundamental component of the anode RF voltage and current are in phase resulting in minimum tube current. In addition the power supply ripple is compensated. The loop is DC coupled with a bandwidth of about 10 kHz.

b. Amplitude Control Loop

This adjusts the RF drive current such that the gap voltage is maintained at the prescribed level under varying beam loading conditions. The loop gain and bandwidth are dependent on the Q of the cavity and unavoidable delays.

c. Radial Loop

This generates a frequency correction in the VCO proportional to the measured radial beam displacement. The measurement is in general somewhat dependent on beam intensity. The loop cut-off frequency must be below the synchrotron frequency.

d. Phase Loop

This controls the phase of the generator current and maintains the relative phase between the gap voltage and beam current constant. The cut-off frequency is greater than the synchrotron frequency to ensure strong damping of dipole mode phase oscillations. The loop gain is limited by the Q of the resonator.

In addition to the above loops a signal is provided to enable the RF system to be phase locked with that of PETRA prior to extraction and transfer. Figures 7.4. and 7.5. show the cavity Q value and synchrotron frequency respectively which govern the design of the loops.

The VCO consists of a combination of a very stable frequency synthesiser and a low noise, fast response analog VCO.

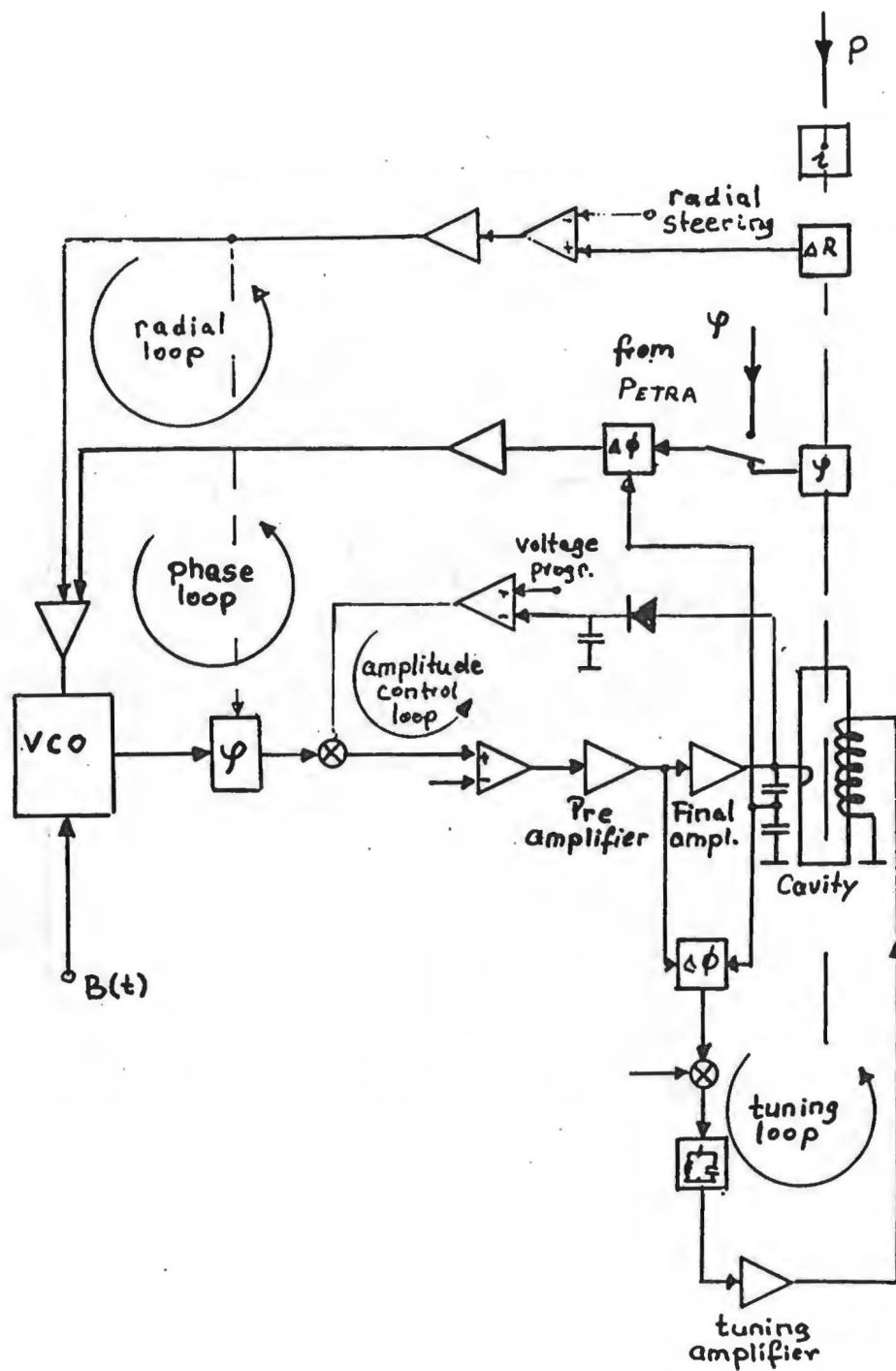


Figure 7.1. RF System Schematic.

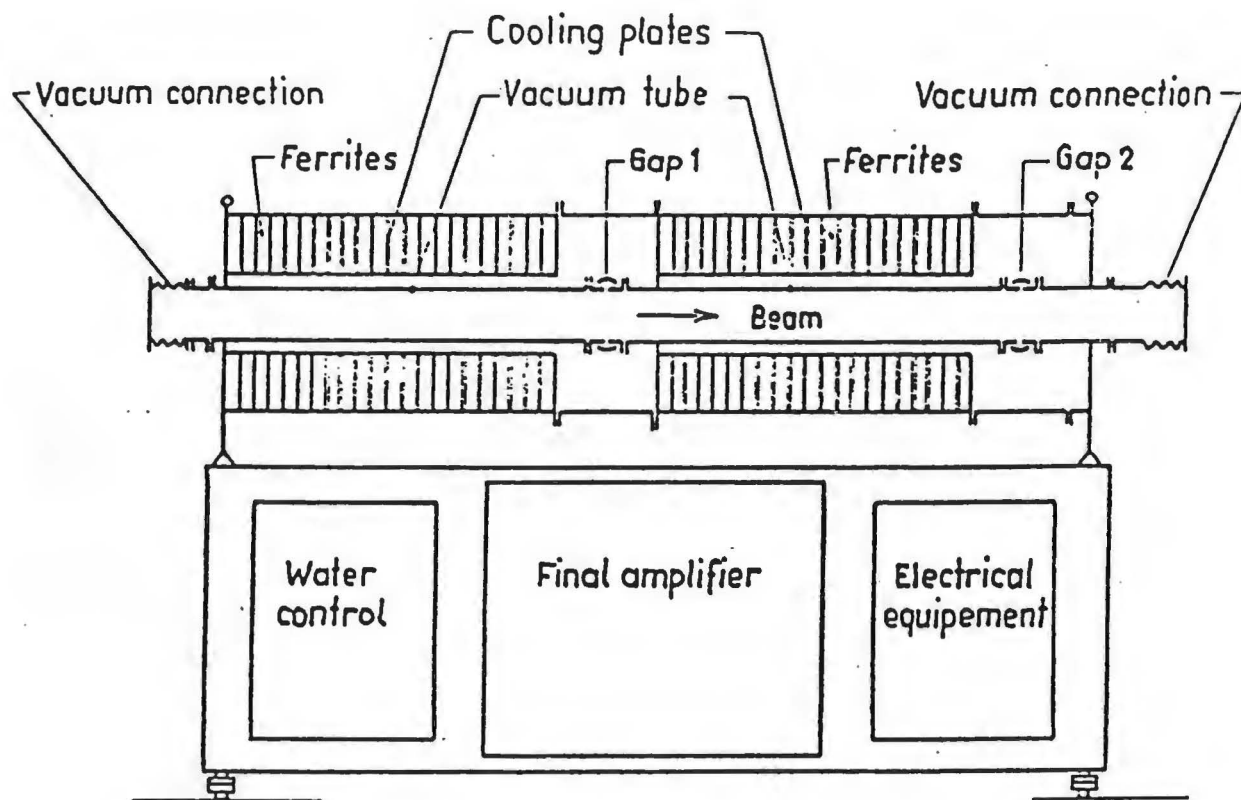


Figure 7.2. RF Cavity.

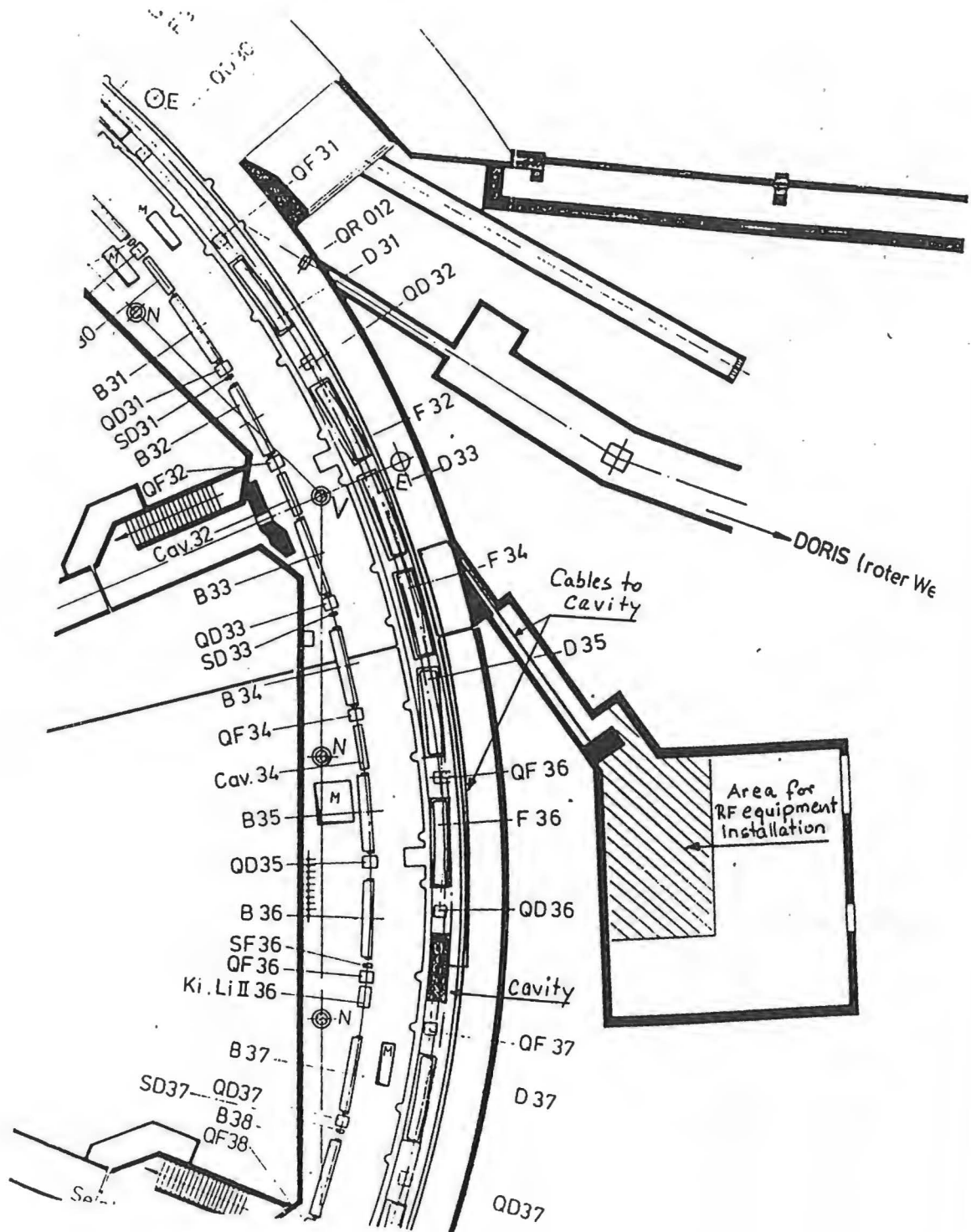


Figure 7.3. RF Region in Hall

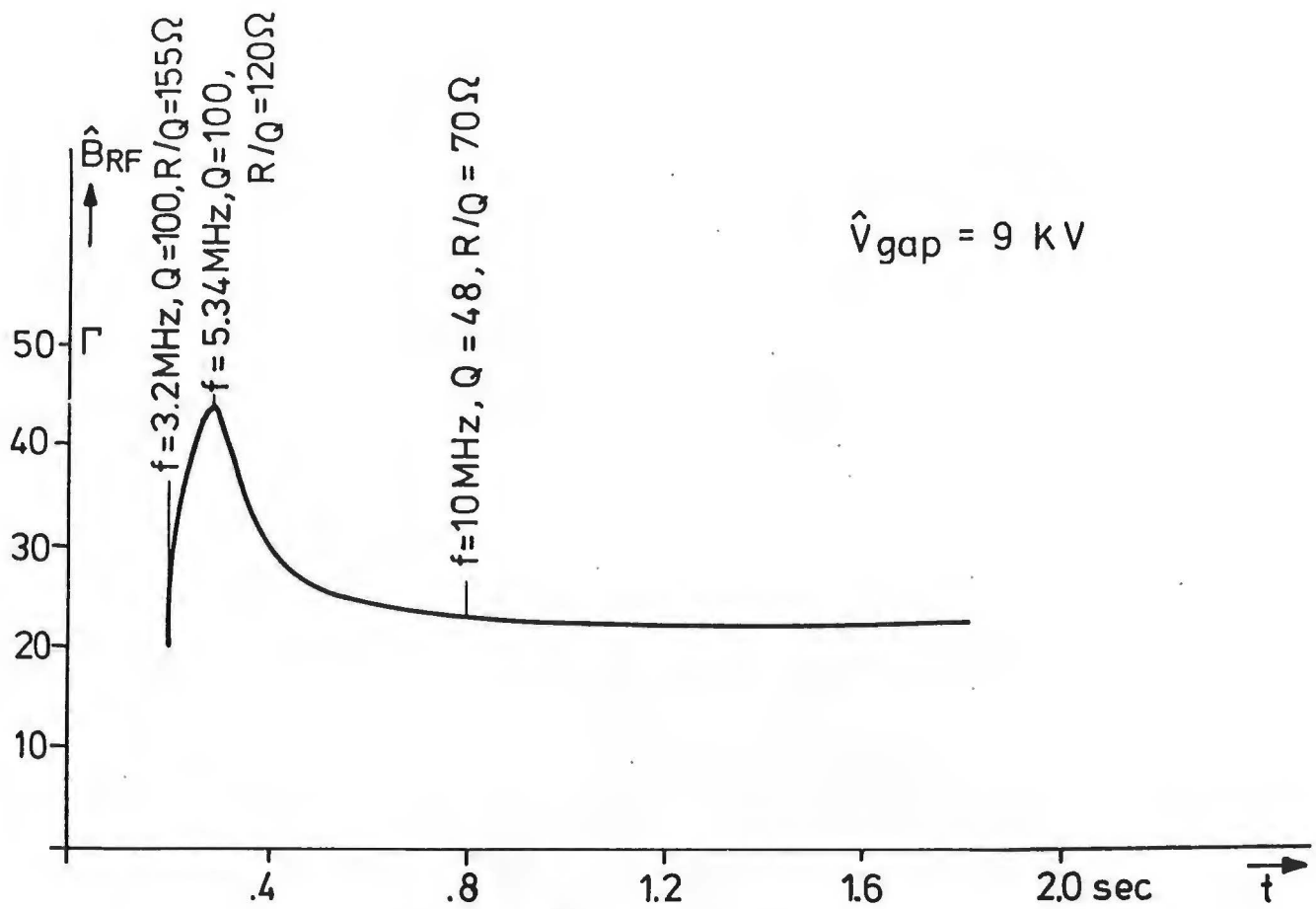


Figure 7.4. RF Induction in Ferrites

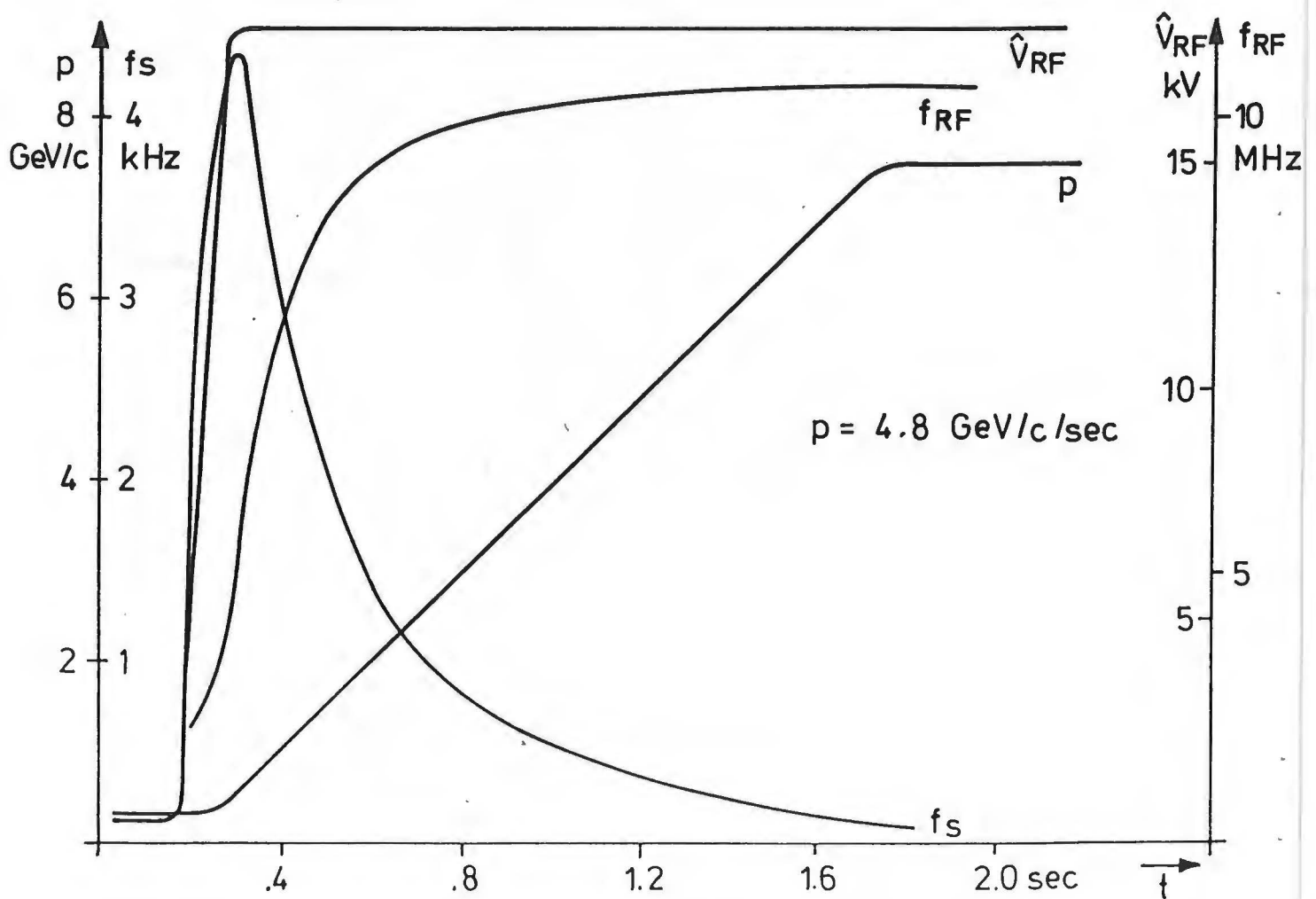


Figure 7.5. RF Parameters versus Time

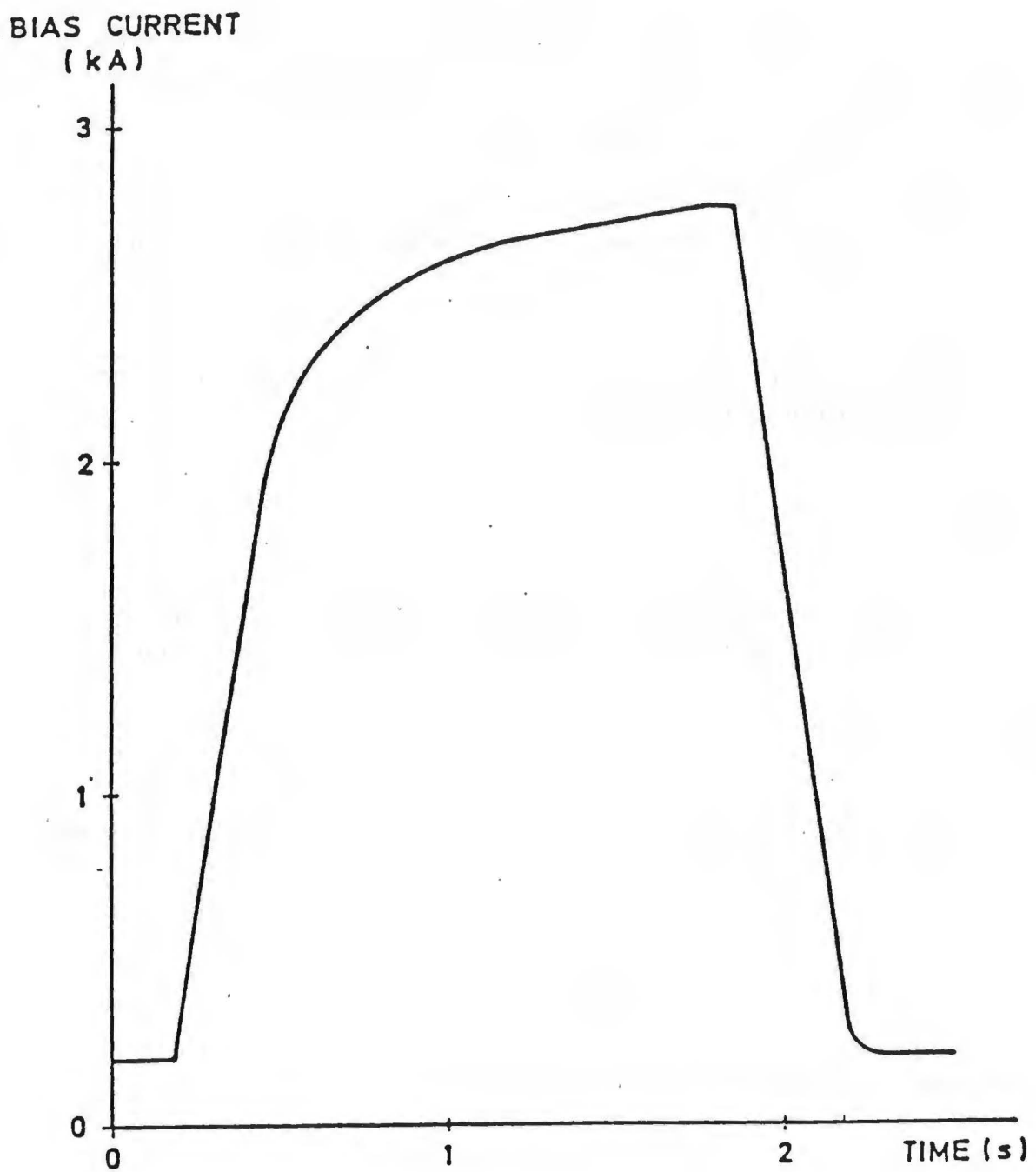


Figure 7.6. Bias Current versus Time

8 Vacuum System.

To achieve stable acceleration of the relatively high proton current the vacuum chamber must be "smooth", i.e. it should present a low impedance to the beam. Because the cycling rate is reduced from 50 Hz to ~ 0.3 Hz we propose to use an all-metal system rather than the somewhat fragile and expensive existing ceramic chambers. An investigation of eddy current effects, the results of which are given in detail below, has shown that the wall thickness may be in the range 1 to 2 mm. The required pressure is specified to be $p \leq 1.5 \cdot 10^{-8}$ mbar. Of possible materials the most favourable, both from the viewpoint of strength and availability, is non-magnetic stainless steel type number 1.4541.

The variation of the magnetic field induces eddy currents in the chamber walls which cause power losses and field distortions. These effects have been calculated. The results are as follows:

Assuming triangular magnet excitation with $B = .525$ T/S corresponding to 5 GeV/c/s we find for the elliptical stainless chamber:

Eddy current losses:

$$\begin{aligned} N'_D &= .07 \text{ Watts/m} & \text{D-chamber } 80 \times 75 \text{ mm}^2 & \quad d = 1 \text{ mm} \\ N'_F &= .08 \text{ Watts/m} & \text{F-chamber } 80 \times 50 \text{ mm}^2 & \quad d = 1.5 \text{ mm} \end{aligned}$$

These losses are negligible.

The field distortions at injection field (321 Gauss) are shown in Figures 8.1. and 8.2.

We find

$$\left(\frac{\Delta B}{B}\right)_F = -1.5 \times 10^{-3}$$

field decrease in the centre of the F-chamber and

$$\left(\frac{\Delta B}{B}\right)_D = -0.76 \times 10^{-3}$$

for the D-chamber.

The sextupole components depend on the shape of the ellipse. For a circle-like chamber the sextupole component vanishes, while for a flat chamber the effect is maximum. We find

$$m_F = \frac{1}{B_0 \rho_0} \frac{d^2 B}{dx^2} = 0.034 m^{-3} \quad d = 1.5 \text{ mm}$$

$$\text{and } m_D = 0.01 m^{-3} \quad d = 1.0 \text{ mm}$$

The change of chromaticity $\Delta\xi_x \simeq +2.3$; $\Delta\xi_z \simeq -2.0$ is small compared with the natural chromaticity

$$\xi_x = -6.14; \xi_z = -5.82$$

The circular cross-section D-chamber ($\phi = 84 \text{ mm}$; wall thickness $s = 1.0 \text{ mm}$) will be installed in the appropriate magnets from the outside ring radius. The F-chamber, with an elliptical cross-section ($b = 83 \text{ mm}$; $h = 51 \text{ mm}$; $s = 1.5 \text{ mm}$), must be positioned by inserting into the magnet from one end and subsequently welding on the flanges. To allow simple demounting of the chambers a multiply re-usable welding lip is provided. The chambers themselves are smooth and follow the orbit curvature. To avoid steps between the round and elliptical profiles, transition tapers will be used.

The D-chambers are equipped with beam position monitors using a 25 mm thick ceramic ring built into the walls. To ensure minimum uncertainty in beam position measurements they are adjacent to the geometrical reference/adjustment point. Here a compensator is provided to ensure correct take-up of the position, angle and installation tolerances as well as allowing for thermal movements. Figure 8.3. shows the arrangement of components at such a point between an F- and D-sector. The chambers are connected together using Conflat-Systems flanges. Each dipole chamber is wrapped with a single layer of Capton foil to ensure electrical isolation from the magnet pole pieces.

The ring is divided into four sections by means of vacuum valves, each section being equipped with a turbo-pump module. The installed ion-getter pumps will ensure that a pressure of 1.10^{-7} mbar is attained after 24 hours. After ten days operation the pressure reduces by an order of magnitude yielding the specified value of $\sim 10^{-8} \text{ mbar}$. The vacuum controls are compatible with those existing in DESY II.

Due to the profile and length variations there are in total five types of chamber including those in the medium and long straight sections. Figure 8.4. is an illustration of an octant showing the various dimensions.

Since the beam elevation in DESY III is coincident with that of DESY II special chambers are needed to accommodate the crossing electron injection and extraction beam paths; in addition five D-sectors (D11, D25, D27, D45, D47) will be bored through.

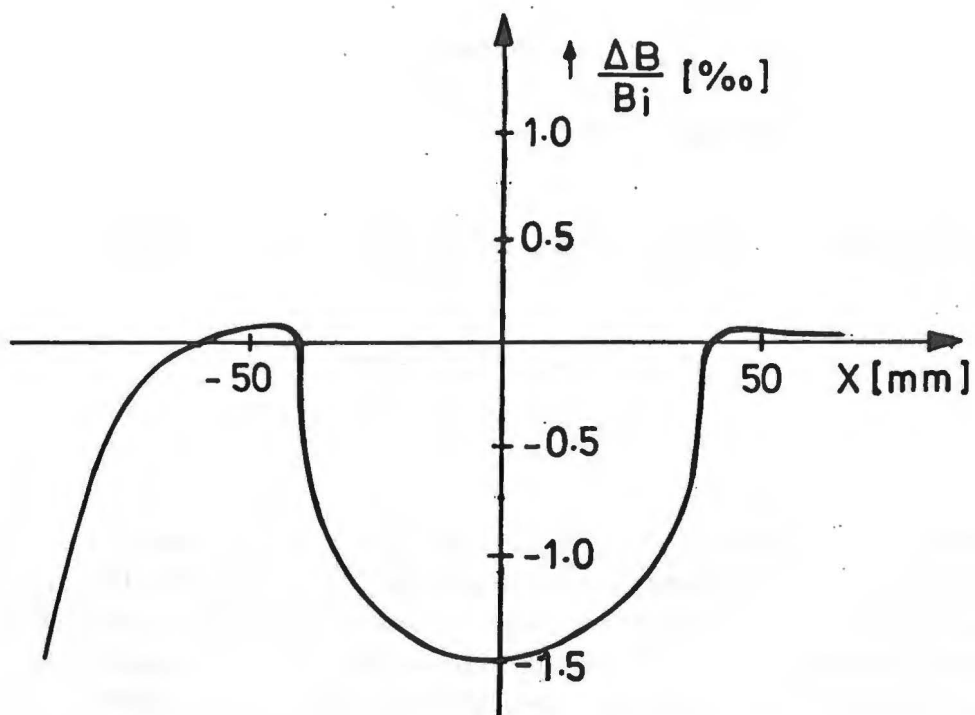


Figure 8.1. F-sector Eddy Current Field Error

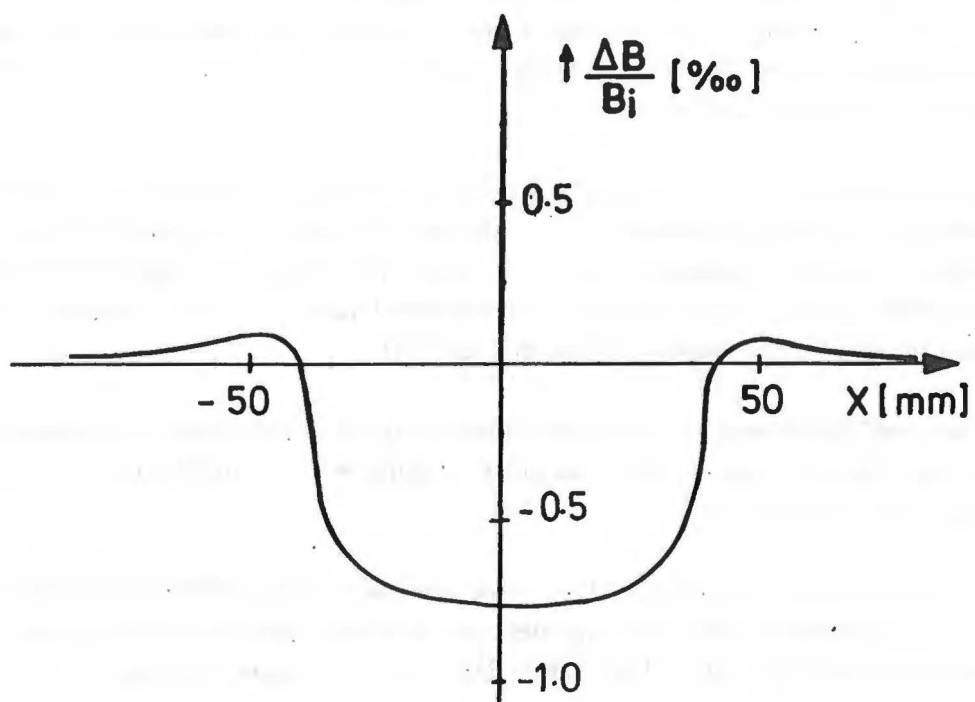


Figure 8.2. D-sector Eddy Current Field Error

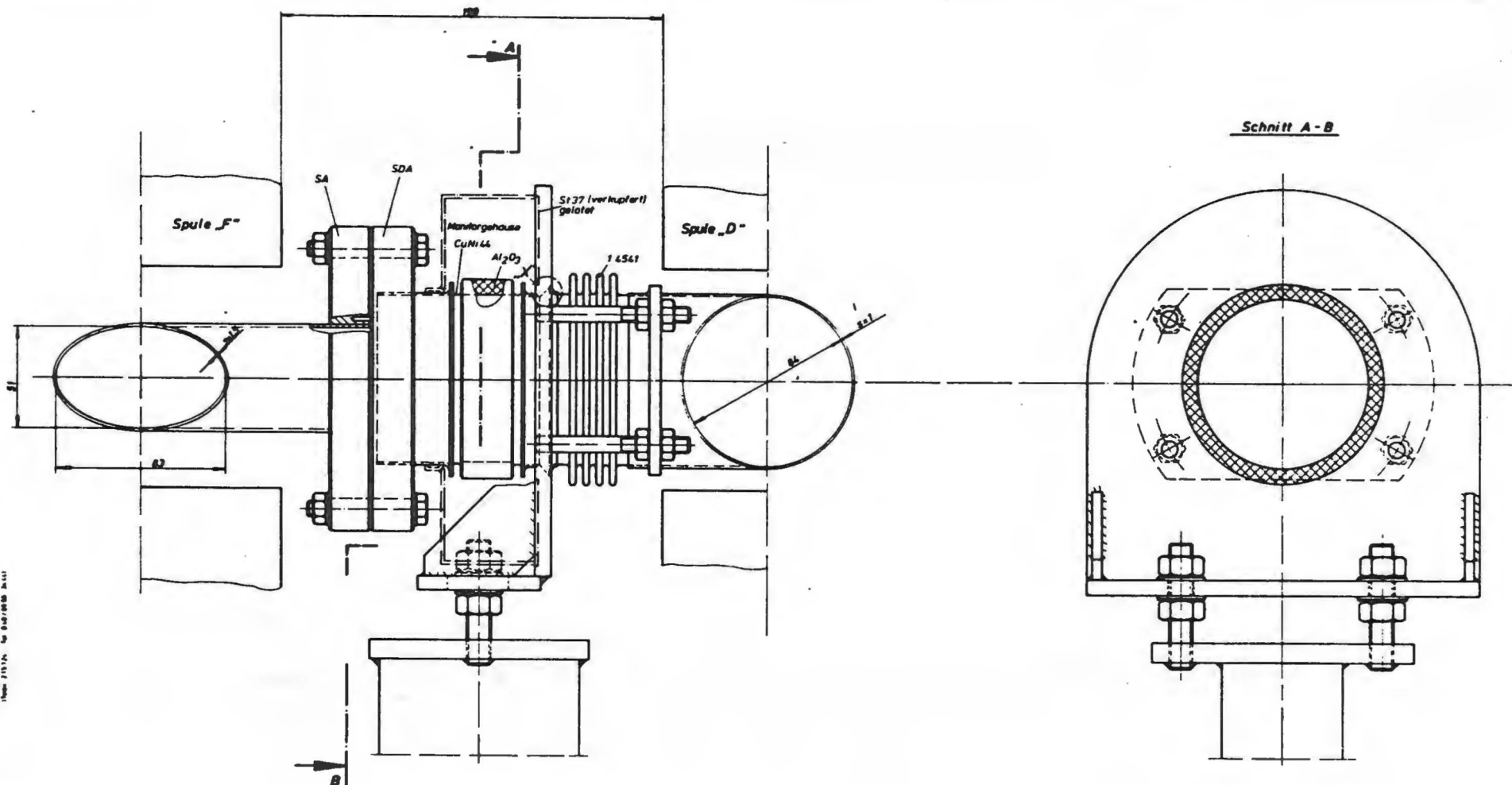


Figure 8.3. Vacuum Components between Sectors

DES Y-Matrix													Teil erscheinend auch in:	
q ₁ (mm)	0,025	0,05	0,1	0,2	0,4	0,8	1,6	3,2	6,3	12,5	25	50	andere Bezeichnung	
q ₂ (mm)	N1	N2	N3	N4	N5	N6	N7	N8	N9	N10	N11	N12	✓	
Matrix 1 (10 1)														
DES Y-PVAC													Dipolzwischenstück Monitorvariante DES Y III	

Uptown 375.8 am

1941
12, 13, 14

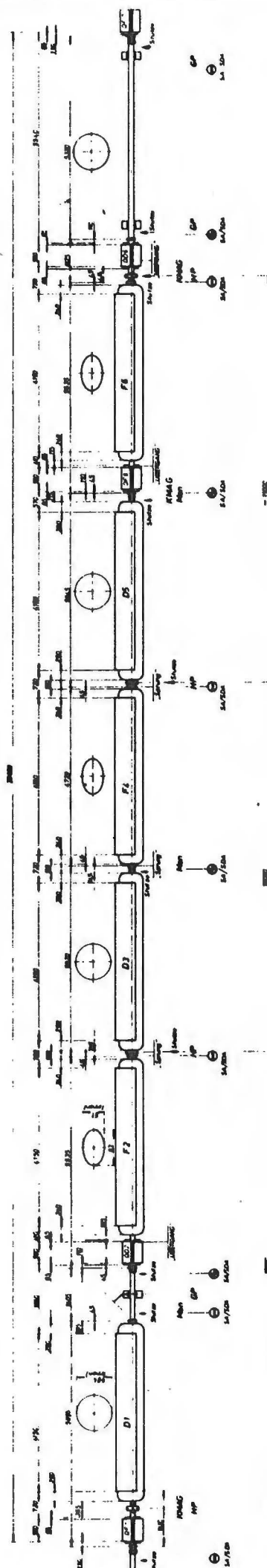


Figure 8.4. Vacuum Components in an Octant

STANDARD 503

[illegible]

10-10-1964

9 Diagnostics.

a. Position Monitors

To measure the transverse beam position around the ring inductive pick-up stations will be used. The required number is ~ 4 per betatron wavelength i.e. $\sim 4 \times Q$ units. Three units per octant will be installed giving a total of 24.

Such pick-up stations exist in DESY I and their characteristics at low frequency (0.3 to 1.0 MHz) have been measured. The monitor sensitivity is 7.5 mV/mA.mm with a resolution of 0.4 mm.mA. Since those installed in DESY III are of similar dimensions we expect to achieve similar values. Some additional magnetic field shielding will be incorporated. The sum of a few of these monitors, equidistantly spaced around the ring, will give a slow radial reference signal to the RF system.

b. Current Measurement

By using the same signal from the electrodes of a position monitor a signal proportional to intensity may be derived. However this is only the case when there is a component of current at the revolution frequency. In order to measure current during injection of an essentially coasting beam a DC-current transformer similar to that operating in the DORIS storage ring will be installed. In either case the signal will be normalized in the computer to $\beta = 1$ using the rise of the magnetic field.

c. Luminescent Screens

Several scintillators will be installed to aid in the initial running-in of the machine and to provide some information where the functioning of other monitors is doubtful. They will be placed close to the injection and extraction azimuth together with a few intermediate positions around the ring. The images will be transmitted to the control room via TV cameras.

d. Wide Band Longitudinal Pick-up

To measure bunch length together with possible longitudinal oscillations and density fluctuations 2 to 4 wide band ≤ 1 GHz pick-up stations will be installed. The station design will be based on that used in the CERN PS-Booster ^[12] consisting of a ceramic insertion in the vacuum chamber bridged by resistors from which coaxial cables lead to a summing network.

The Booster pick-up has a sensitivity of 5.5 V/A with a rise time of 380 ps corresponding to a bandwidth of 900 MHz. The low frequency cut-off is ~ 100 kHz.

As all elements are outside the vacuum chamber, modifications e.g. to trade sensitivity against bandwidth, may be easily made. These pick-ups will also be used in the phase regulation loop of the RF system.

e. Q-Measurement

To measure the number, Q , of betatron oscillations per revolution the beam is excited to perform coherent transverse oscillations whose frequency is measured together with the RF frequency. The coherent oscillations contain the frequencies:

$$f_m = |m - Q|f_{rev}, \quad m = 0, \pm 1, \pm 2 \dots$$

The amplitude of the mode m depends on $|m - Q|$, the shape of the kick in time and on the ratio $\Delta t/\tau$ of its duration to the revolution period. To obtain signals from the position monitors which are independent of momentum the kick amplitude must increase proportionally to the bending field and $\Delta t/\tau$ has to be kept constant.

The kicker, designed to excite either radial or vertical oscillations, may consist of 8 conductors parallel to the beam arranged in a common vacuum vessel. It may also be used to investigate the coupling between the transverse planes and to blow up the beam in a controlled manner.

f. Emittance Measurement

Two types of monitors can be used, horizontal and vertical wire scanners or a secondary electron emission grid (SEM). To deduce the emittance in both planes 2 x three of either type are required one being placed at a beam waist and the other two positioned 120° in betatron phase upstream and downstream of the first. SEM grids will also be used in the transfer lines.

g. Loss Monitors

Monitors will be installed to indicate beam loss in specific critical places, e.g. injection and extraction azimuths. A good time resolution (~ 10 ns) is needed to study the loss mechanism in detail. A combination of scintillator and photomultiplier is the obvious choice.

10 Power Supplies.

The specified main bending field versus time may be seen in Figure 10.1. This form of field rise must be followed by the 4 independent quadrupole circuits with some allowance for individual programming to provide a facility for varying the betatron tunes etc. At 7.5 GeV/c the nominal current in each circuit should be:

Dipole	1250 A
Quadrupole QF	1220 A
Quadrupole QD	990 A
Quadrupole QF1	280 A
Quadrupole QD1	190 A

The current ramps in all 5 circuits will be generated by thyristor controlled power supplies which allow operation either as converters or as inverters. Converters are required for the current increase and flat top whilst inverters are used to create the negative voltage and energy return needed to create the linear fall. We shall refer to these power supplies as Type I. A typical voltage versus time variation in such a supply is shown in Figure 10.2.

The injection platform, of duration 0.2 s within the overall 3.6 s cycle, will be generated in each circuit by the use of additional DC current sources - Type II. This arrangement can satisfy the specified relative variation of the cycle to cycle injection field value ($\Delta B/B \sim \pm 2 \times 10^{-4}$) when the current is only $\sim 4\%$ of that at full energy.

The power supplies for injection and ramping/flat top may be series or parallel switched. In the first case there is a free wheeling diode at the output of the injection supply, rated at the full magnet current. In the second case the supplies may be connected via 2 diodes. The first case gives better grounding conditions with the small power supplies arranged between the two parts of the larger one.

The number, type and DC power rating of the proposed power supplies is shown in Table 10.1. Instead of four different types of quadrupole power supplies we provide only two with unregulated currents of 1220 and 280 Amps respectively.

Table 10.1 Power Supplies Required

Circuit	No.	Type	Power	
Dipole	1	I _D	1300	kW
Dipole	1	II _D	2	kW
Quadrupole	2	I _{Q1}	76	kW
Quadrupole	2	II _{Q1}	0.3	kW
Quadrupole	2	I _{Q2}	6.5	kW
Quadrupole	2	II _{Q2}	0.1	kW

Each type I unit will be equipped with thyristors for 12-pulse rectification and will contain passive filters capable of reducing the 600 Hz ripple voltage by a factor of 15. During the flat top the expected peak-peak ripple currents are then:

Dipole circuit	15 mA
Quadrupole circuit 1	50 mA
Quadrupole circuit 2	50 mA

For the dipole circuit this ripple represents a relative variation of the peak current of $< \pm 1 \times 10^{-5}$ whilst for the quadrupoles the relative deviation in tracking the dipoles is $< \pm 1 \times 10^{-3}$ as specified. In this fashion the use of active filters may be avoided.

For control purposes the computer will provide 3 reference values:

- a.) A constant reference for current setting at flat bottom using the type II dipole circuit unit.
- b.) A time varying value used to set the voltage of the type I dipole unit during both the rising and falling field ramps ('Voltage program').
- c.) A constant reference value for flat top current regulation of the type I dipole unit.

The digital references will be transformed to analogue values using DACs and switched on and off at the correct times. They will be further processed in the voltage or current regulation circuits of the dipole units. The 4 quadrupole currents will follow the dipole current using differential DC current transformers. These measure a (suitable) difference between the current in each quadrupole circuit and that in the defining dipole circuit. The difference is nullified via the current regulation circuits of the quadrupole units to within a relative error of $\sim \pm 1 \times 10^{-3}$.

The difference between the PETRA dipole current and the DESY III dipole current will be formed in a similar fashion and used as a correction value for the DESY III dipole current regulation.

Triggering the thyristors creates reactive power and voltage reduction in the mainly inductive AC mains reactances which, because of the ramping operation, is a time varying situation. A reduction of this effect may be achieved by connecting a fast, variable inductance (3-phase, thyristor controlled choke) to the rectifier unit's mains clamps. This ensures that the total inductance is held constant. If the existing reactive power compensation of the DESY 10 kV AC mains supply is insufficient there must be further compensation using capacitors and additional chokes.

During the time variation of the primary current, phase variations will appear on the 10 kV mains voltage. The magnitude and effect of this phase jitter, e.g. on the DESY II circuits, must be investigated. If necessary the DESY III primary supply must be derived from a separate 10 kV mains system, which is less sensitive to phase jitter.

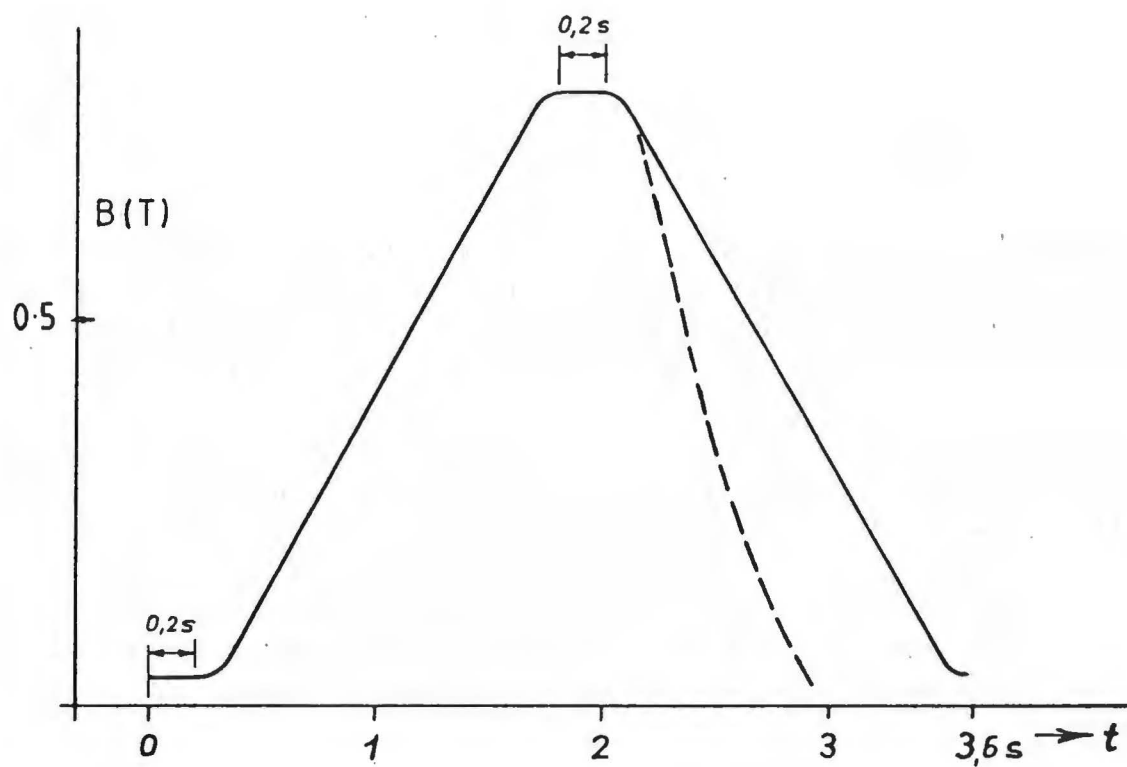


Figure 10.1. Bending Field versus Time

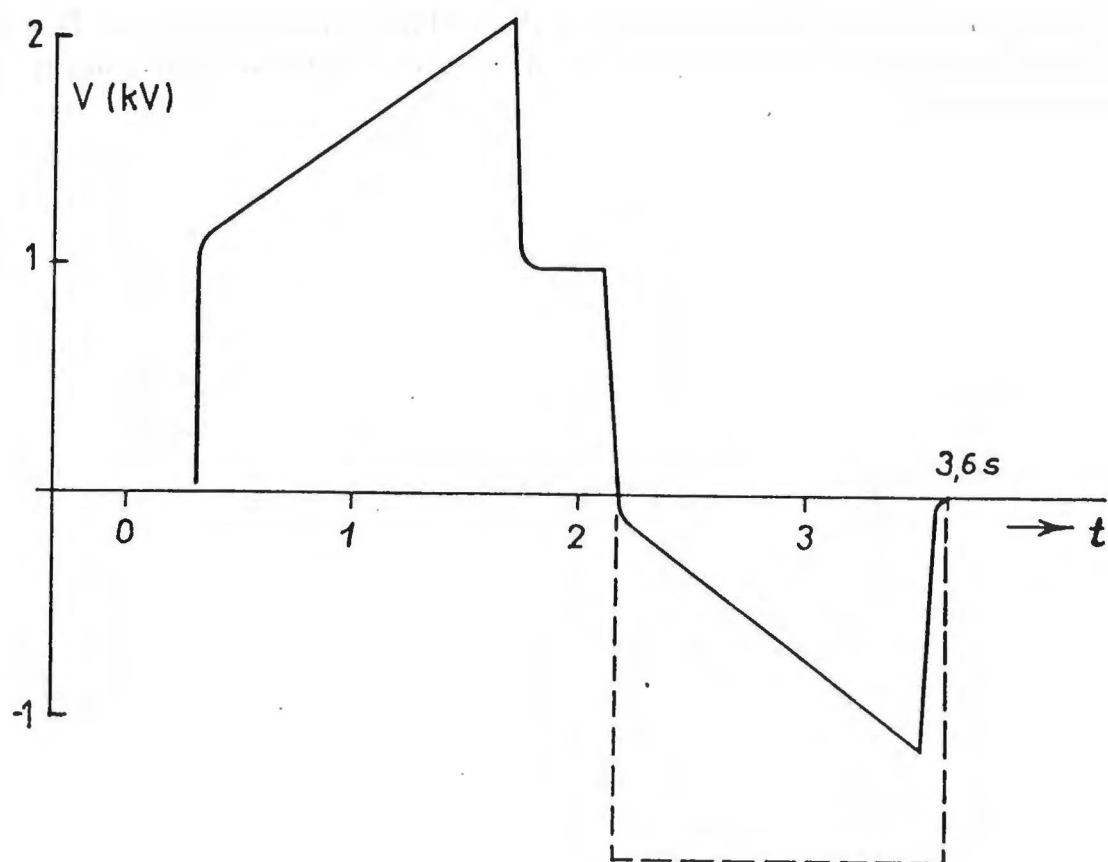


Figure 10.2. Power Supply Volts versus Time

11 Controls.

The control system for DESY III is based closely on that in use at PETRA and employed in DESY II. Operator instructions are input in the control room via the general purpose console connected to a mini computer. The console contains a touch panel, to allow menu-selectable choice of procedures, together with a number of TV screens for data display.

Many of the accelerator systems have their own local controls using micro computers. The interface between each equipment control module and the main computer uses PADAC and SEDAC standards. Where possible the applications software will be written in the high level interactive language POCAL. System status will be monitored on a regular basis, the information being stored in a common database which may, for example, be interrogated by the the display processors to produce a TV picture of the current status of a chosen system. In addition watchdog programs will monitor the information and report on equipment malfunction.

Specific tasks such as orbit measurement will have access to a file store so that sets of data taken at different times may be saved for subsequent recall and analysis. In this way information such as the orbit variation within the acceleration cycle or on a longer term pulse to pulse history may be derived.

The advantage of close compatability with the PETRA system lies not only in the standardisation of much of the hardware and software, but also in that it permits flexible use of operations manpower.

12 Construction.

The process of machine construction is conveniently divided into two phases. Firstly the dismantling of the existing DESY I ring and secondly, after modification of those components which will be re-used, the installation of the DESY III systems.

It is necessary to bore through the yokes of 5 D-sectors as listed below:

D11 for the P-Weg (e^+) to PETRA.

D25 for the γ -test beam 22.

D27 for the γ -test beam 24.

D45 for the G-Weg (e^+) to DORIS.

D47 for the E-Weg (e^-) to PETRA.

The remaining beams to and from DESY II cross in straight sections. The geometry of each crossing point is detailed in Figures 12.1. to 12.4.

All of the upper water pipes which form part of the ring carrier thermal stabilisation system will be removed since tests have shown they are not needed. This will leave a flat surface which will ease installation. The magnet stands will be modified, being provided with a 3-point support system using new feet. Figure 12.5 is a sketch showing the new foot at one end of a magnet together with the associated load spreading plate. The stands will, upon re-installation in their new positions, be glued to the ring carrier.

Stress analysis has shown that the torsion applied to the carrier by the redistribution of the magnets may be safely withstood however, should it be wished to provide a greater factor of safety, some of the magnets could be provided with additional supports by means of pillars based on the foundation in the cellar. Such a support is shown in Figure 12.6.

The time shedule for the dismantling phase is shown in Table 12.I.

The installation phase has access to the synchrotron hall limited by planned operation of DESY II in April 1987 and mid-June to mid-July 1987. Installation of the magnet stands, magnets and quadrupoles is scheduled for the period between the two DESY II runs thus allowing some time for the ring carrier to settle prior to accurate alignment of the elements. The quadrupole stands are based on those used for DESY II but of the correct height. A sketch of such a stand may be seen in Figure 12.7.

The installation schedule is shown in Table 12.II. Testing of the complete ring with beam may commence in October 1987.

Table 12.I. DESY III Construction 1986/7


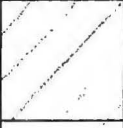

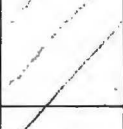


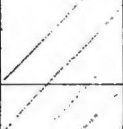
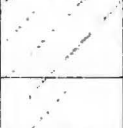
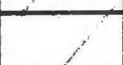





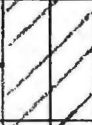





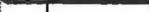






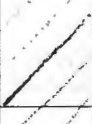


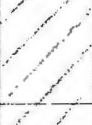
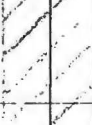

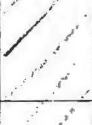





ITEM	Nov 86	Dec 86	Jan 87	Feb 87	Mar 87	Apl 87
Remove Magnets	_____					
Dismantle Straights	_____					
Refurbish Magnets	_____	_____	_____	_____		
Clear Carrier	_____					
Remove Upper Pipes		_____				
Bore 5 Magnets			_____	_____		
Measure Magnets			_____	_____	_____	
Mark Out Carrier		_____	_____			
Install F-Chambers					_____	

Table 12.II DESY III Construction 1987

ITEM	Apl	May	June	July	Aug	Sept	Oct	Nov	Dec
Install Magnet Stands									
Install Magnets									
Install RF System									
Align Magnets									
Install Vacuum System									
Install Injection System									
Install Ejection System									
Connect Services									
Connect Control Cables									
Start Tests									

Crossing point No. 1

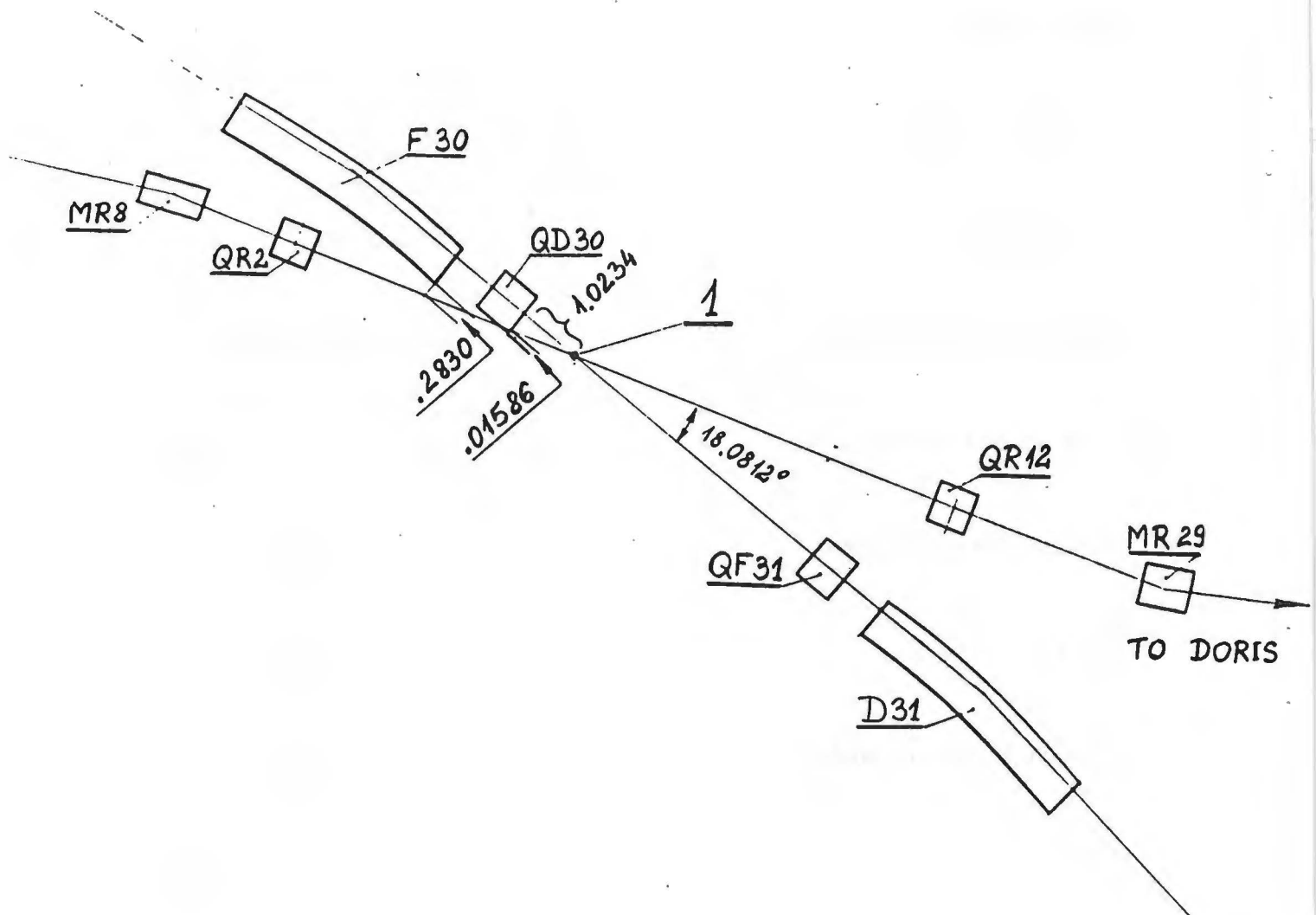


Figure 12.1. Crossing Point Geometry

Crossing points No. 2 and 3

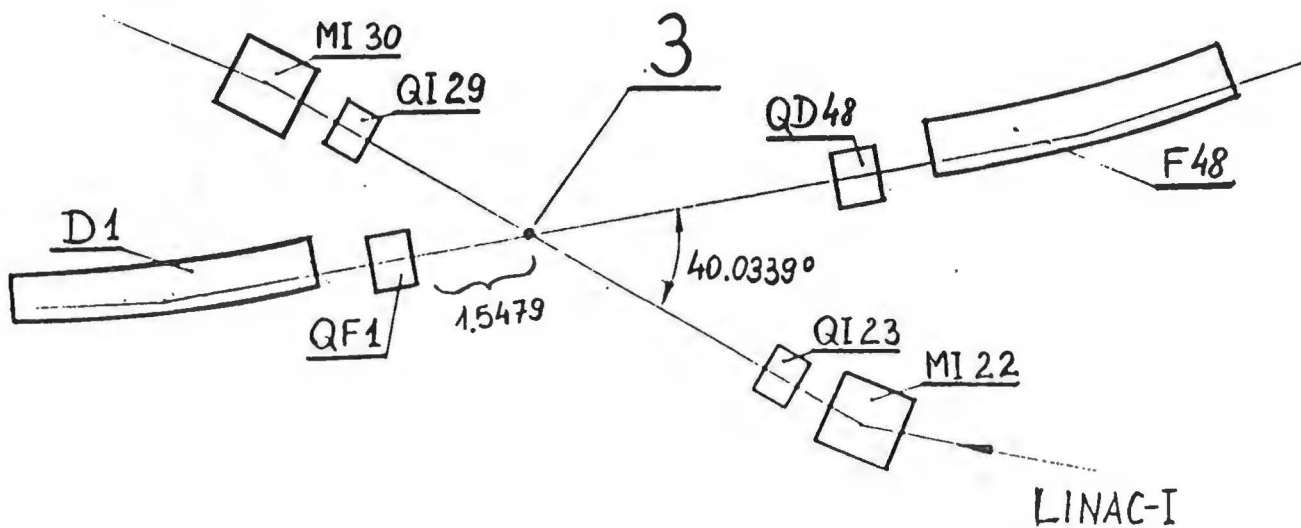
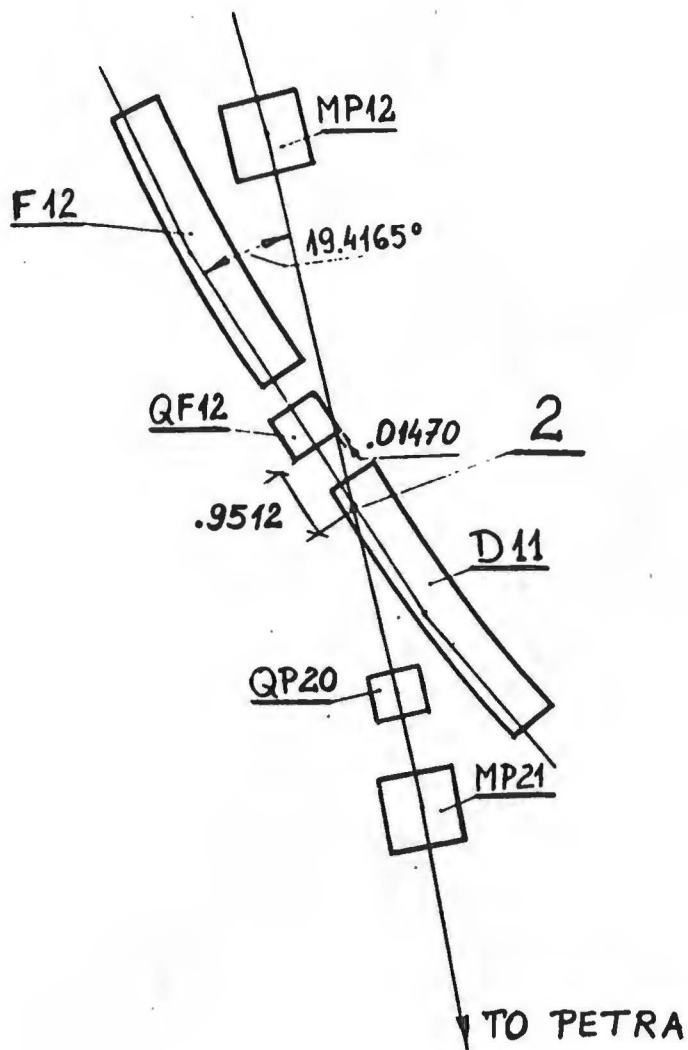


Figure 12.2. Crossing Point Geometry (cont.)

Crossing points No. 4 and 5

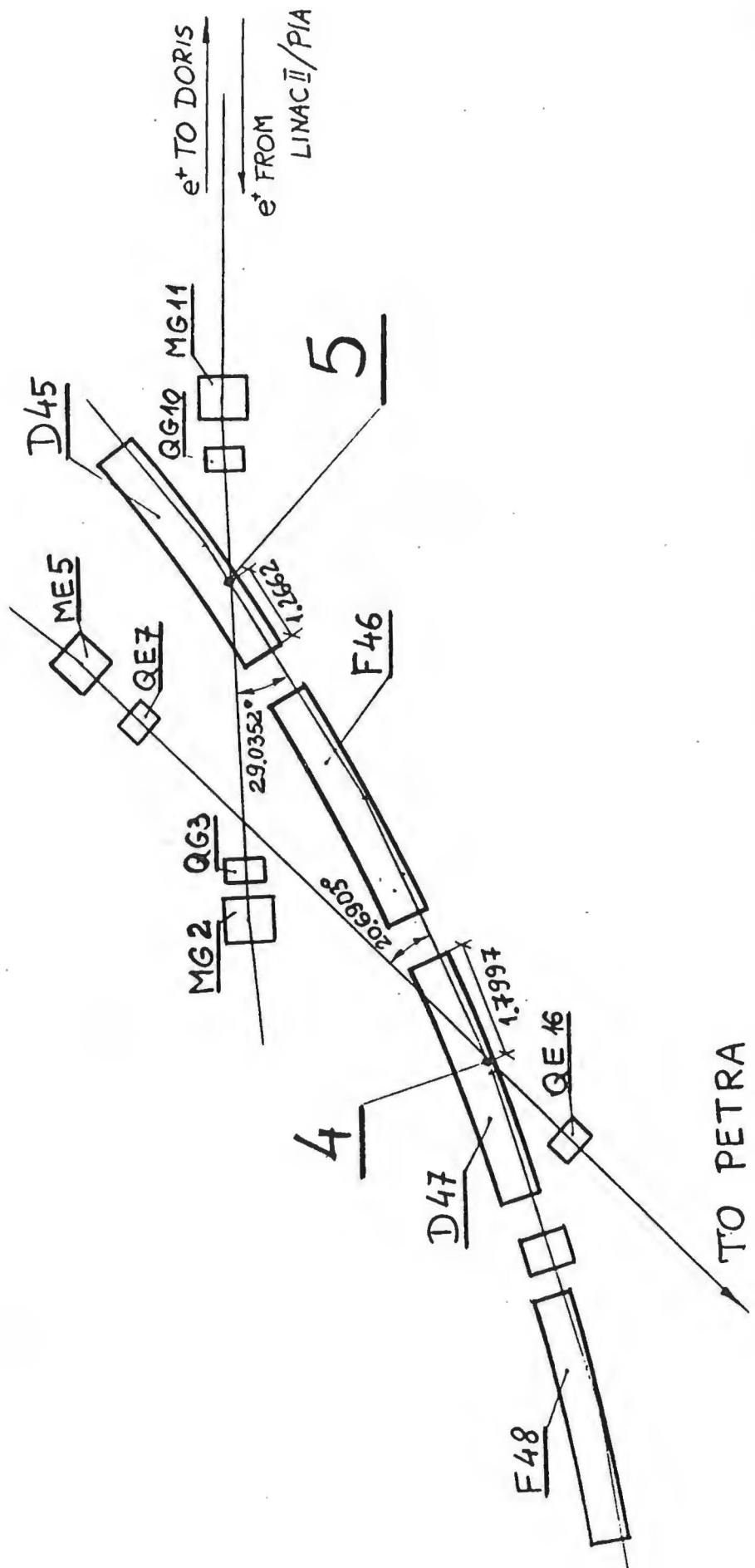


Figure 12.3. Crossing Point Geometry (cont.)

Crossing point No. 6

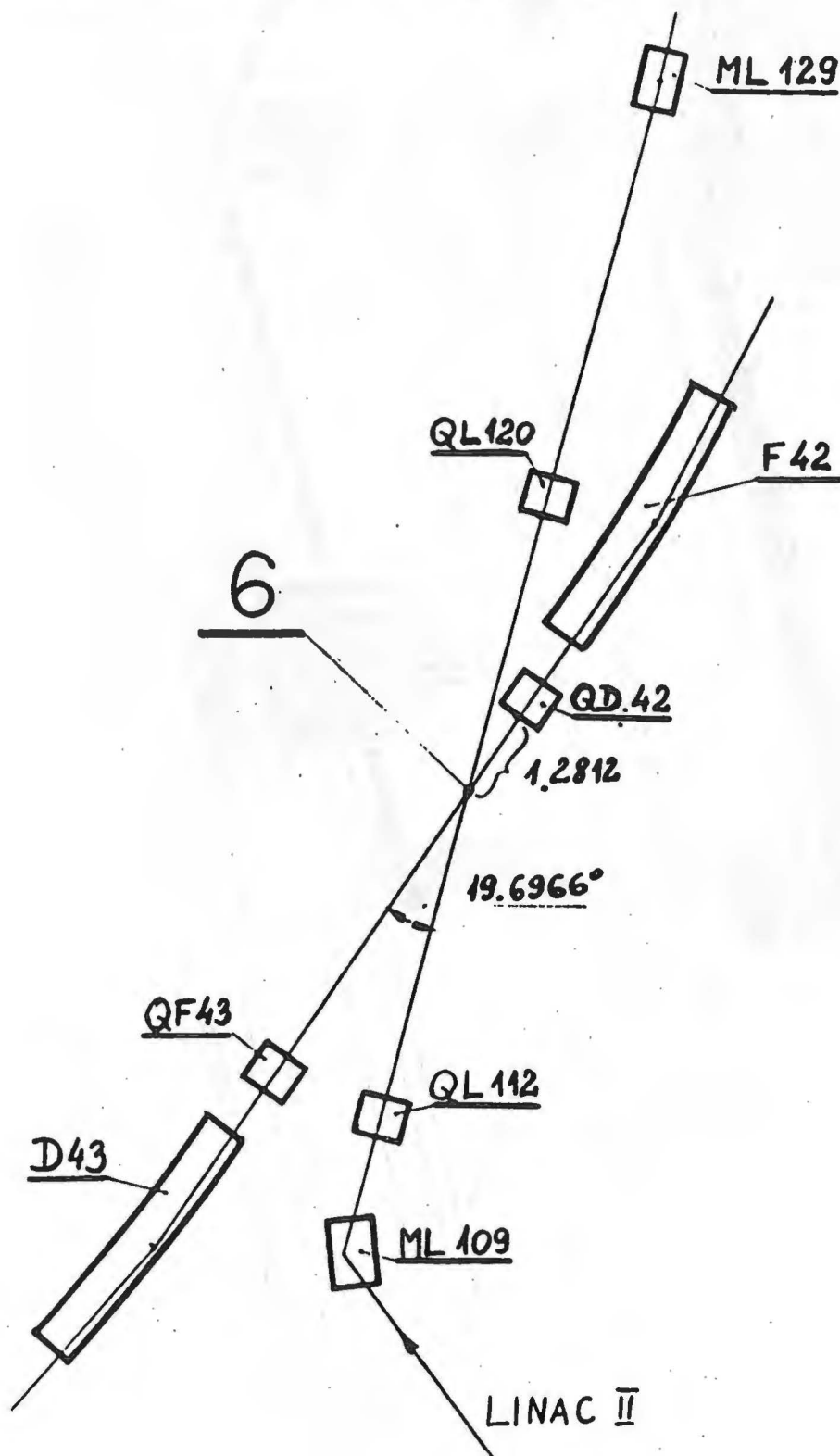


Figure 12.4. Crossing Point Geometry (cont.)

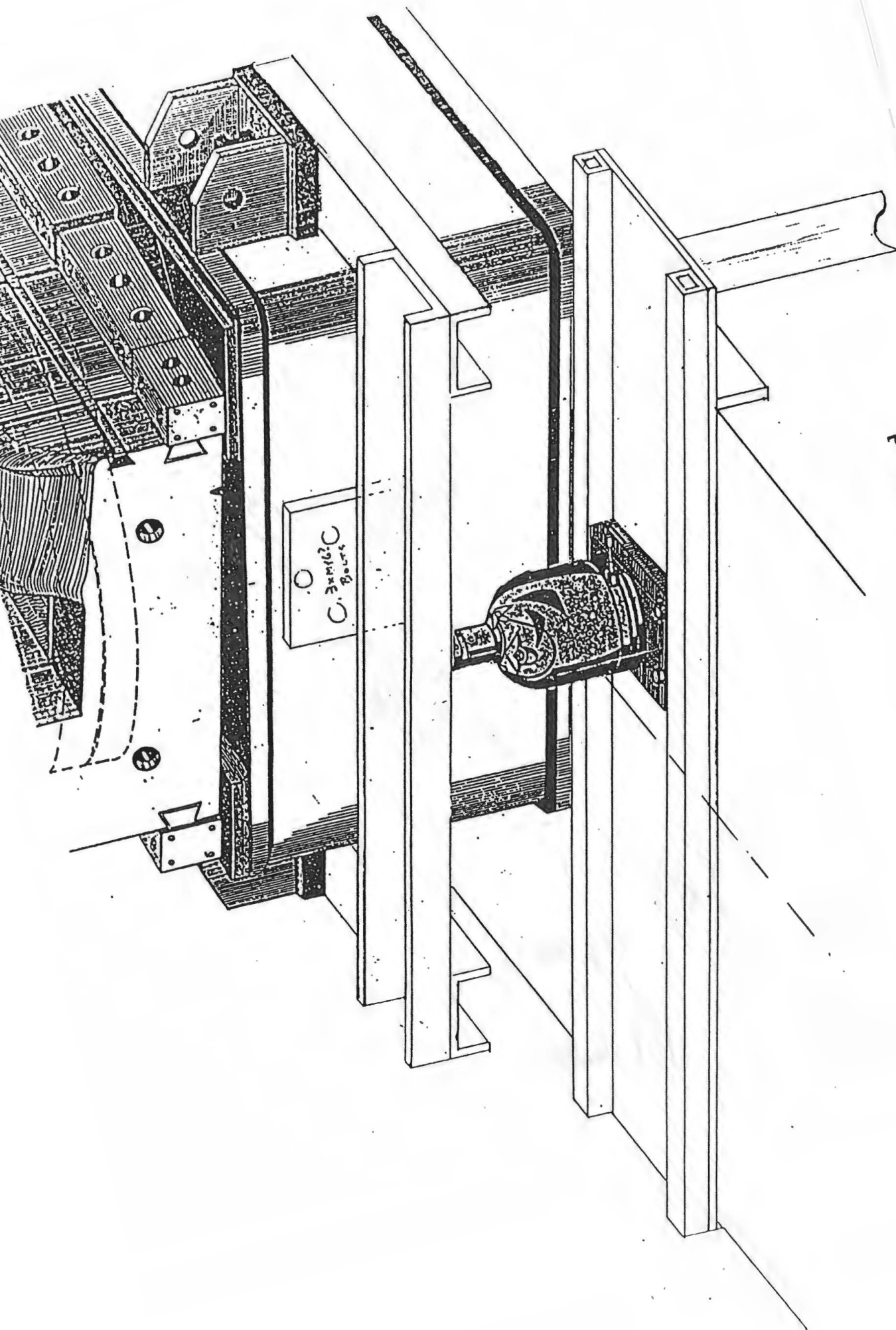


Figure 12.5. Foot for Magnet Stand

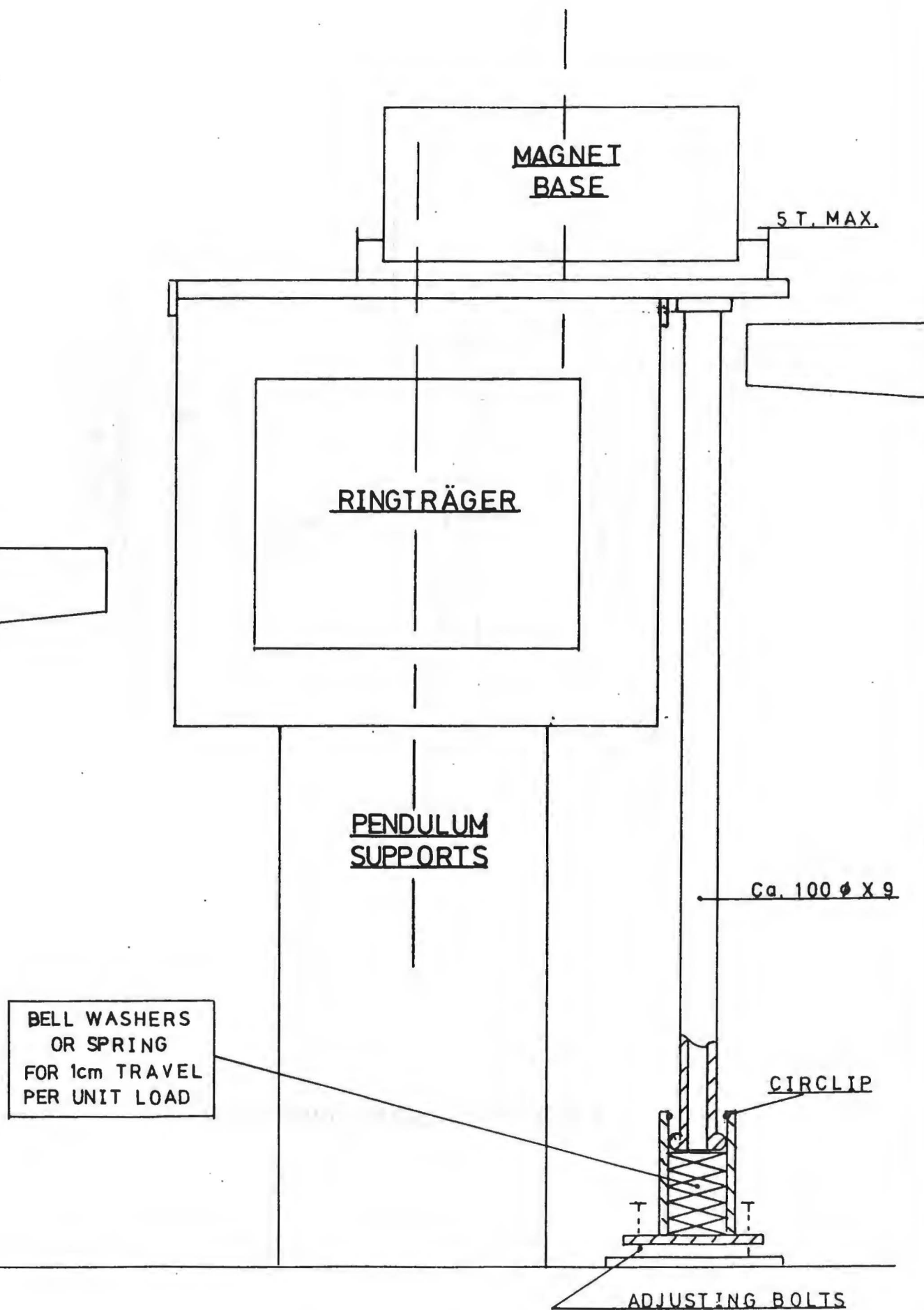


Figure 12.6. Torsion Compensation (if required)

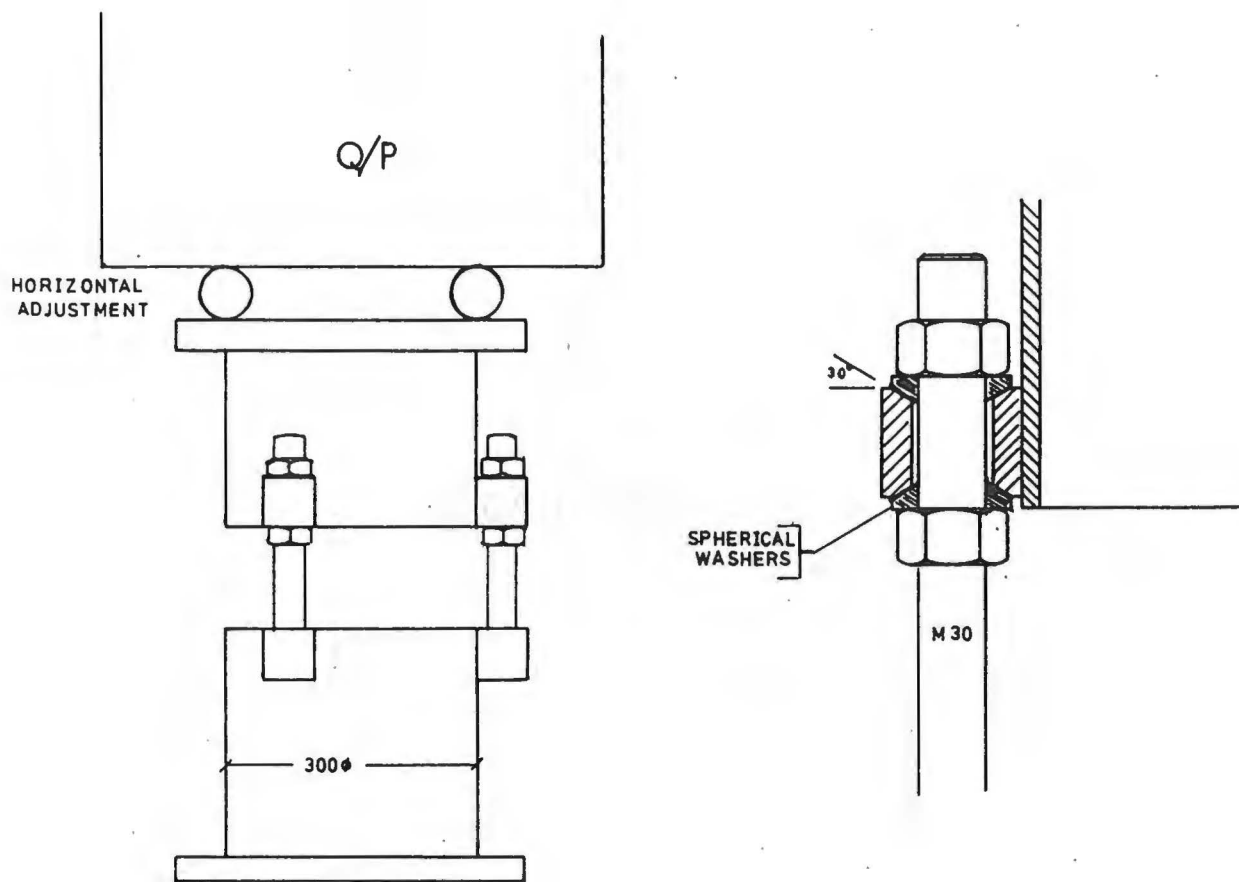


Figure 12.7. Quadrupole Stand

13 References

- 1) J.R.Maidment, DESY/HERA 84-08
- 2) U.Timm (Ed.), DESY/HERA 84-12
- 3) E.Karantzoulis, J.R.Maidment, DESY/HERA 86-01
- 4) F.Schmidt, DESY/HERA 86-10
- 5) A.Wrulich, DESY 84-026
- 6) R.Meinke, Private communication
- 7) D.Boussard, CERN LAB II/RF/Int/75-2
- 8) H.Hereward, CERN/ISR-DI/75-47
- 9) G.Nassibian, CERN/PS 84-25 (BR)
- 10) M.Gygi-Hanney et al., CERN/LEP-TH/83-2
- 11) C.S.Biddlecombe et al., RL 81-089
- 12) H.Koziol, K.H.Reich, IEEE Trans. on Nucl. Sci., Vol NS-18, No. 3, p 347 (1971)